

Novel Hyperelastic Models for Large Volumetric Deformations

Kevin M. Moerman^{a,b,**}, Behrooz Fereidoonnezhad^a, Patrick McGarry^{a,*}

^a*National University of Ireland Galway, Galway, Ireland*

^b*Massachusetts Institute of Technology, Cambridge, MA, United States of America*

Abstract

Materials such as elastomeric foams, lattices, and cellular solids are capable of undergoing large elastic volume changes. Although many hyperelastic constitutive formulations have been proposed for deviatoric (shape changing) behaviour, few variations exist for large deformation volumetric behaviour. The first section of this paper presents a critical analysis of current volumetric hyperelastic models and highlights their limitations for large volumetric strains. In the second section of the paper we propose three novel volumetric strain energy density functions, which: 1) are valid for large volumetric deformations, 2) offer separate control of the volumetric strain stiffening behaviour during shrinkage (volume reduction) and expansion (volume increase), and 3) provide precise control of non-monotonic volumetric strain stiffening. To illustrate the ability of the novel formulations to capture complex volumetric material behaviour they are fitted and compared to a range of published experimental data.

Keywords: Hyperelasticity, Volumetric Deformation, Finite Strain, Strain Energy Density, Shrinkage, Expansion

*Corresponding author

**Corresponding author

Email addresses: kevin.moerman@nuigalway.ie (Kevin M. Moerman), patrick.mcgarry@nuigalway.ie (Patrick McGarry)

1 1. Introduction

2 Foams, lattices, and cellular materials are common in nature and engi-
3 neering applications [1, 2, 3, 4]. Given the large elastic volume changes these
4 materials can undergo [5], accurate descriptions of material behaviour be-
5 yond the small strain domain is required. Such behaviour may include an
6 asymmetric shrinkage-expansion response in addition to a highly non-linear
7 pressure-volume relationship.

8 Hyperelastic continuum models offer a convenient means to model the
9 large strain mechanical behaviour of complex materials. However, although
10 the hyperelasticity literature is rich in terms of variations in modelling of
11 the deviatoric (shape changing) material response, as evident from the many
12 different formulations which have been proposed (e.g. close to a hundred
13 described in a recent review [6]), few variations exist for modelling the volu-
14 metric contribution (e.g. [7, 8, 9, 10]).

15 The goal of this study is to provide novel volumetric strain energy formu-
16 lations which: 1) are valid for large volumetric deformations, and 2) enable
17 the separate control of volumetric strain-dependent stiffening during shrink-
18 age (volume reduction), and expansion (volume increase).

19 Accurate modelling of the volumetric behaviour of materials like soft
20 foams and lattices is of interest since it is relevant to the design of support
21 structures (see review [11]), such as foam cushions and seats [12, 13, 14, 15],
22 helmets [16], and shoes and insoles ([17, 18, 19]). Furthermore compliant lat-
23 tices and foams are also employed in the design of soft robotics [20, 21, 22, 23].
24 Recent advances in material science include the development of ceramic
25 nanolattices [24], mycelium-based bio-foams [25], ultraporous sponges [26]
26 graphene foams and aerogels (e.g [27, 28, 29, 30]) some capable of recovering
27 from 90% compression [31]. Furthermore, accurate volumetric formulations
28 are relevant to stroke biomechanics research since blood clot contractions
29 cause large volume changes (e.g. possibly over 80% volume loss [32]).

30 Hyperelastic constitutive formulations have their origins in the modelling
31 of rubber [33, 34, 35, 36]. Although rubber is most commonly modelled as in-
32 compressible (no volume change), it does present with a non-linear pressure-
33 volume response during large deformation hydrostatic compression (20% vol-
34 ume reduction [36]), and volumetric hyperelastic formulations capturing this
35 behaviour have been proposed (e.g. [7]). These, as we will show here, are
36 however not generally valid for very large hydrostatic compression.

37 Hyperelasticity is also commonly used for soft tissues (see review [6]).

38 However, like with rubbers, these are often assumed to be incompressible or
 39 nearly-incompressible. For these applications the volumetric contributions
 40 are commonly considered largely as a simple penalty term to enforce (near)
 41 incompressibility (e.g. [37, 38]), rather than a topic of detailed investigation.
 42 Consequently the formulations used for these volumetric contributions are
 43 often not valid for very large volume changes. For foams and highly com-
 44 pressible materials the so called hyperfoam formulation [8, 39, 40]) is common
 45 (see for instance [41, 17, 42, 43, 44, 14]). However, we show here it is not
 46 robustly designed for very large volume changes.

47 The first part of this study is a critical analysis of current volumetric
 48 hyperelastic formulations, and presents a discussion of their limitations for
 49 large volumetric deformations and non-linear applications. In the second
 50 part of this study three novel volumetric strain energy formulations are pre-
 51 sented (and several variations in the appendix) which offer validity for large
 52 volumetric strains as well as flexibility for experimental fitting of complex
 53 behaviour for both the shrinkage and expansion domain. In addition, the
 54 third formulation was expanded to include non-monotonic volumetric strain
 55 stiffening (e.g. potentially leading to a plateau in the observed stress) as
 56 seen for crushable foams and cellular materials. Finally, the models are com-
 57 pared to experimental data for neoprene rubber foam [45], flexible open-cell
 58 polyurethane cushioning foam [17], natural cork [46], and rigid closed-cell
 59 polyurethane foam [47].

60 2. Theoretical background and rationale

61 In hyperelasticity the constitutive behaviour, i.e. the material's stress-
 62 strain behaviour, is derived from a formulated strain energy density (SED)
 63 function (for a more detailed discussion of these concepts the reader is re-
 64 ferred to established text-books on the subject [48] and [35]). In the case
 65 of uncoupled formulations the strain energy consists of additive deviatoric
 66 (shape changing) $\Psi_{dev}(\tilde{\mathbf{C}})$ and volumetric (volume changing) $\Psi_{vol}(J)$ contri-
 67 butions:

$$\Psi(\tilde{\mathbf{C}}, J) = \Psi_{dev}(\tilde{\mathbf{C}}) + \Psi_{vol}(J) \quad (1)$$

68 Here $\tilde{\mathbf{C}}$ and J represent the deviatoric right Cauchy-Green tensor and the
 69 volume ratio (or Jacobian), respectively. This leads to an additive decoupling
 70 of the stress tensor, such that

$$\boldsymbol{\sigma} = \boldsymbol{\sigma}_{dev} + \sigma_h \mathbf{I} \quad (2)$$

71 where $\boldsymbol{\sigma}_{dev}$ is the deviatoric stress tensor, σ_h is the scalar hydrostatic stress,
 72 and \mathbf{I} is the identity tensor. σ_h is given as

$$\sigma_h = \frac{1}{3} \text{tr}(\boldsymbol{\sigma}) = -p \quad (3)$$

73 where $p = -\sigma_h$ is commonly referred to as the pressure. For an un-coupled
 74 formulation, σ_h is determined from the volumetric component of the strain
 75 energy density, such that

$$\sigma_h = \frac{\partial \Psi_{vol}(J)}{\partial J} \quad (4)$$

76 This paper focuses on the analysis and development of volumetric strain
 77 energy density formulations for large volumetric deformations. We consider
 78 both volume reduction ($J < 1$) and volume increase ($J > 1$), referred to as
 79 *shrinkage* and *expansion*, respectively.

80 Although many formulations have been proposed for deviatoric strain en-
 81 ergy contributions Ψ_{dev} (see for instance the review article [6]), relatively
 82 few formulations have been proposed for the volumetric strain energy contri-
 83 butions $\Psi_{vol}(J)$ (for a more detailed discussion of volumetric strain energy
 84 formulations the reader is referred to the surveys by Doll and Schweizerhof
 85 [10] and Horgan and Murphy [49]). Moreover, volumetric components of
 86 hyperelastic models are not typically subjected to rigorous analysis in or-
 87 der to ensure that physically realistic behaviour for large volume changes is
 88 maintained. The study of Doll and Schweizerhof [10] establishes 9 criteria
 89 (summarised as *I-IX* in Table 1) that should be satisfied in order to ensure
 90 physically realistic material behavior during expansion and shrinkage. Here
 91 we add a tenth (*X* in Table 1), namely: the volumetric component of a hy-
 92 perelastic model should be capable of precisely describing strain stiffening
 93 for all values of J (shrinkage and expansion).

Table 1: Validity and consistency criteria for $\Psi_{vol}(J)$

| id | Description | Form |
|-------------|---|--|
| <i>I</i> | Zero SED in reference state | $\Psi_{vol}(J = 1) = 0$ |
| <i>II</i> | Zero hydrostatic stress in reference state | $\sigma_h(J = 1) = 0$ |
| <i>III</i> | Positive strain energy density | $\Psi_{vol}(J \neq 1) > 0$ |
| <i>IV</i> | Consistent with linear elasticity | $\frac{d^2\Psi_{vol}(J=1)}{dJ^2} = \kappa$ |
| <i>V</i> | SED approaches ∞ if J approaches 0 | $\lim_{J \rightarrow 0} \Psi_{vol}(J) = \infty$ |
| <i>VI</i> | Hydrostatic stress approaches $-\infty$ if J approaches 0 | $\lim_{J \rightarrow 0} \sigma_h(J) = -\infty$ |
| <i>VII</i> | SED approaches ∞ if J approaches ∞ | $\lim_{J \rightarrow \infty} \Psi_{vol}(J) = \infty$ |
| <i>VIII</i> | Hydrostatic stress approaches ∞ if J approaches ∞ | $\lim_{J \rightarrow \infty} \sigma_h(J) = \infty$ |
| <i>IX</i> | Tangent modulus > 0 (polyconvexity) | $\frac{d^2\Psi_{vol}(J)}{dJ^2} \geq 0$ |
| <i>X</i> | Control of strain stiffening for all J | |

94 *2.1. Structure of this paper*

95 The current paper is structured as follows.

96 In Section 3 we analyze the capability of four existing models to satisfy
97 the criteria set out in Table 1:

- 98 • In Section 3.1 commonly implemented single parameter models are
99 analysed;
- 100 • In Section 3.2 the formulation by Bischoff et al. [7] for hydrostatic
101 compression of rubber is analysed;
- 102 • In Section 3.3 we analyse the modified Ogden formulation [9, 50], a
103 simplified form of which has been implemented in ABAQUS® (2018,
104 Dassault Systèmes Simulia Corp.);
- 105 • In Section 3.4 we analyse the Ogden-Hill hyperfoam formulation [8],
106 which has been implemented in ABAQUS®, for highly compressible
107 elastomers;
- 108 • In Section 3.5 we analyze the model of Doll and Schweizerhof [10].

109 In Section 4 we propose three novel formulations that improve upon existing
110 formulations in terms of the criteria outlined in Table 1:

- 111 • In Section 4.1 we expand the single parameter model (of Equation 6)
112 to fulfil all criteria of Table 1, and to provide independent control of
113 strain stiffening in shrinkage and expansion;

- 114 • In Section 4.2 we present a formulation that facilitates precise prescrip-
 115 tion of "lock-up" strains in expansion and shrinkage;

 116 • In Section 4.3 we expand the model presented in Section 4.2 to also cap-
 117 ture non-monotonic strain stiffening (typically observed in elastomeric
 118 foams).

119 This paper focuses on volumetric strain energy density formulations for
 120 large volumetric deformations. Properties of several commonly used forms
 121 are discussed and three novel formulations are proposed. Although the ar-
 122 guments are most readily presented using uncoupled formulations, they can
 123 be extended to coupled formulations where the effective volumetric response
 124 can also be separately identified.

125 All visualizations presented here were created based on the free and open
 126 source MATLAB® (R2019a, The MathWorks Inc., Natick, MA, USA) tool-
 127 box GIBBON (<https://www.gibboncode.org>, [51, 52]). Readers interested in
 128 exploring MATLAB® implementations, and associated visualizations, of all
 129 discussed formulations presented here, may explore the following demo which
 130 was added to GIBBON as part of this study: DEMO_volumetric_SED_eval.m.

131 **3. Review and critical analysis of current volumetric SED formu-**
 132 **lations**

133 *3.1. Common single parameter volumetric SED formulations*

134 Two commonly used forms for $\Psi_{vol}(J)$, in particular for uncoupled for-
 135 mulations, are (e.g. [53]):

$$\Psi_{vol}(J) = \frac{\kappa}{2} \ln(J)^2 \quad (5)$$

136 and (e.g. [54, 55]):

$$\Psi_{vol}(J) = \frac{\kappa}{2}(J - 1)^2 \quad (6)$$

137 These are featured in many finite element implementations such as the
 138 open source package FEBio [56] and the proprietary software ABAQUS®.
 139 These formulations have largely been used to model materials that are as-
 140 sumed to be nearly incompressible (such as rubbers and soft tissues), for
 141 which $J \approx 1$. The motivation for these formulations stems largely from their
 142 mathematical convenience. Although their performance when $J \approx 1$ is valid,
 143 as we shall describe shortly, non-physical behaviour occurs for large volume

144 changes. Table 1 lists several validity constraints (see also [10, 35]) imposed on
 145 volumetric strain energy density formulations. Doll and Schweizerhof [10] ex-
 146 amined common formulations and showed that equation 5 does not conform
 147 to criteria *VIII* (for high expansions the stress approaches 0 rather than ∞)
 148 and criteria *IX* (for expansion the stiffness reduces to zero at $J = e \approx 2.718$
 149 after which it becomes negative for $J > e$). These effects are summarised in
 150 Figure 1.

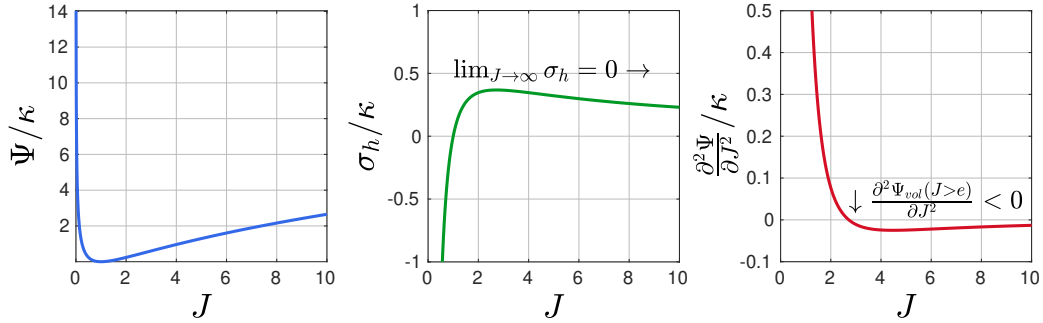


Figure 1: The normalized strain energy density (left), hydrostatic stress (middle), and tangent modulus (right), for the formulation of equation 5

151 Furthermore it was demonstrated that equation 6 does not conform to
 152 criteria *V* (for high shrinkage Ψ_{vol} approaches $\kappa/2$ rather than ∞) and crite-
 153 ria *VI* of Table 1 (for high shrinkage σ_{vol} approaches $-\kappa$ rather than $-\infty$).
 154 These effects are summarised in Figure 2.

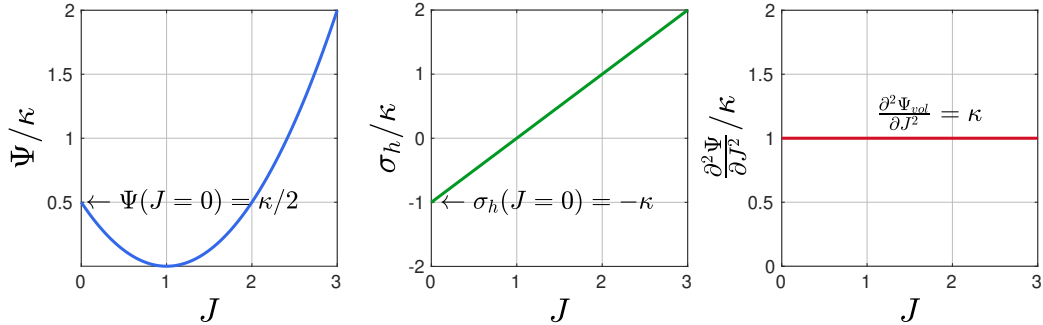


Figure 2: The normalized strain energy density (left), hydrostatic stress (middle), and tangent modulus (right), for the formulation of equation 6

155 For constitutive modelling of rubber-like materials and soft tissues, near
 156 incompressibility, i.e. $J \approx 1$, is a common assumption, hence the above issues

157 associated with large volumetric strains can be avoided. However, when
 158 modelling of compressible material behaviour is of interest, the constraints
 159 need to be satisfied.

160 Finally, these formulations exhibit one fixed type of strain dependent
 161 behaviour and asymmetry in terms of the difference between shrinkage and
 162 expansion, and therefore these formulations do not conform to criteria *X* of
 163 Table 1.

164 *3.2. The Bischoff formulation*

165 Bischoff et al. [7] presents what can be considered a higher-order repre-
 166 sentation of equation 6:

$$\Psi_{vol}(J) = \frac{\kappa}{\alpha^2} \left(\cosh(\alpha(J-1)) - 1 \right) = \kappa \sum_{m=1}^{\infty} \frac{\alpha^{2(m-1)}}{(2m)!} (J-1)^{2m} \quad (7)$$

167 Where α is an additional material parameter. Bischoff et al. [7] demonstrates
 168 a good fit to the experimental hydrostatic compression data for rubber up
 169 to 20%. However, this formulation, and related polynomial forms, have the
 170 same pitfalls as the form of equation 6, i.e. they present with a finite strain
 171 energy, and hydrostatic stress for $J = 0$, thereby violating criteria *V* and *VI*
 172 of Table 1. Furthermore, this formulation does not offer independent control
 173 of the behaviour for shrinkage and expansion, and therefore criteria *X* of
 174 Table 1 is not met.

175 *3.3. The modified Ogden formulation*

176 The modified Ogden formulation [50, 9] is given by:

$$\Psi_{vol}(J) = \frac{\kappa}{\beta^2} \left(J^{-\beta} - 1 + \beta \ln(J) \right) \quad (8)$$

177 , with κ the bulk modulus and β (with $\beta \neq 0$) a material parameter con-
 178 trolling the degree of non-linearity. The hydrostatic stress can be derived
 179 as:

$$\sigma_h(J) = \frac{\kappa}{\beta J} (1 - J^{-\beta}) \quad (9)$$

180 and the tangent modulus:

$$\frac{\partial^2 \Psi}{\partial J^2} = \frac{\kappa}{\beta J^2} \left((\beta + 1) J^{-\beta} - 1 \right) \quad (10)$$

181 Figure 3 below illustrates the behaviour of this formulation for shrinkage
 182 and expansion and for a range of positive and negative β values. In Ogden
 183 [9] the formulation is presented in relation to volume reductions only, and
 184 with $\beta > 0$. However, these restrictions are not generally enforced, and if
 185 $\beta = -2$ is chosen this formulation reduces to the volumetric contribution,
 186 implemented in ABAQUS®, for the uncoupled Aruda-Boyce [57] and Van
 187 der Waals [58, 59] formulations. For shrinkage this formulation presents
 188 with suitable behaviour. For this domain increasing β results in an increase
 189 in strain stiffening. Reducing β has the opposite effect with severely negative
 190 values even inducing a stiffness reduction and a plateauing behaviour (e.g.
 191 see graph for $\beta = -15$ in Figure 3). By studying equation 8 and Figure 3
 192 it becomes clear this formulation does not conform to all criteria of Table 1
 193 in the expansion domain. Specifically if $\beta \geq -1$ the tangent tends to zero
 194 (i.e. $\lim_{J \rightarrow \infty} \frac{d^2\psi_{vol}(J)}{dJ^2} = 0$), and negative tangents occur if $\beta > -1$ (e.g. see
 195 graphs for $\beta = 2$ and $\beta = 15$ in Figure 3), thereby violating criteria *VII*,
 196 *VIII* and *IX*. Furthermore, since this formulation does not offer independent
 197 control over the response for shrinkage and expansion, it does not conform
 198 to criteria *X* of Table 1.

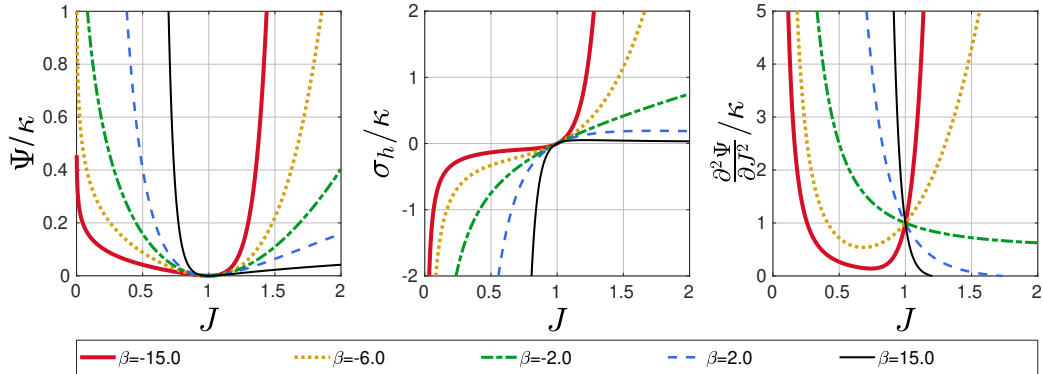


Figure 3: The normalized strain energy density (left), hydrostatic stress (middle), and tangent modulus (right), for the Ogden formulation. Curves drawn for $J = [0, 2]$, $\kappa = 1$, and $\beta = [-15, 15]$

199 3.4. The hyperfoam formulation

200 A popular (see for instance [41, 17, 42, 43, 44, 14]) formulation for mod-
 201 elling of highly compressible materials is the so called Ogden-Hill or *hyper-*
 202 *foam* material implemented in ABAQUS®. The formulation, (see [8], [39]

²⁰³ page 48, and developments in [40]) is given by:

$$\Psi(\lambda_1, \lambda_2, \lambda_3, J) = \sum_{a=1}^N \frac{2\mu_a}{\alpha_a^2} \left(\lambda_1^{\alpha_a} + \lambda_2^{\alpha_a} + \lambda_3^{\alpha_a} - 3 + \frac{1}{\beta_a} (J^{-\alpha_a \beta_a} - 1) \right) \quad (11)$$

²⁰⁴ Here μ_a and α_a are Ogden-like [35, 9] hyperelastic parameters, and β_a enables
²⁰⁵ additional enhancement of volumetric contributions.

²⁰⁶ To review the properties of this formulation we restrict ourselves to a first
²⁰⁷ order formulation ($N = 1$). Furthermore, for volumetric deformations, one
²⁰⁸ may use the conditions $\lambda_1 = \lambda_2 = \lambda_3 = J^{-\frac{1}{3}}$, reducing equation 11 to:

$$\Psi(J) = \frac{2\mu}{\alpha^2} \left(3(J^{\frac{\alpha}{3}} - 1) + \frac{1}{\beta} (J^{-\alpha\beta} - 1) \right) \quad (12)$$

²⁰⁹ The bulk modulus for this formulation is derived from:

$$\kappa = \mu \left(\beta + \frac{1}{3} \right) \quad (13)$$

²¹⁰ Therefore, to ensure $\kappa > 0$ one obtains the constraint $\beta > -\frac{1}{3}$. Furthermore,
²¹¹ from equation 11, it is clear that $\beta_a \neq 0$ is also a constraint. From equation
²¹² 12 the hydrostatic stress can be derived as:

$$\sigma_h(J) = J^{-1} \frac{2\mu}{\alpha} (J^{\frac{\alpha}{3}} - J^{-\alpha\beta}) \quad (14)$$

²¹³ and the tangent modulus:

$$\frac{\partial^2 \Psi}{\partial J^2} = J^{-2} \frac{2\mu}{\alpha} \left(\left(\frac{\alpha}{3} - 1 \right) J^{\frac{\alpha}{3}} + (\alpha\beta + 1) J^{-\alpha\beta} \right) \quad (15)$$

²¹⁴ Although this formulation is reported to be valid in the domain $-\frac{1}{3} <$
²¹⁵ $\beta < 0$ several issues were revealed in this study. As shown in Figure 4, in
²¹⁶ this domain one encounters a reduction in the tangent modulus eventually
²¹⁷ creating negative volumetric stiffness. Furthermore, the stress may reduce
²¹⁸ to 0 as $J = 0$ is approached. It was found that the effect is exacerbated by
²¹⁹ the parameter α , therefore even if a negative β is chosen close to 0 (which
²²⁰ appears to provide valid behaviour in Figure 4) a negative stiffness may still
²²¹ occur if the α parameter is sufficiently high.

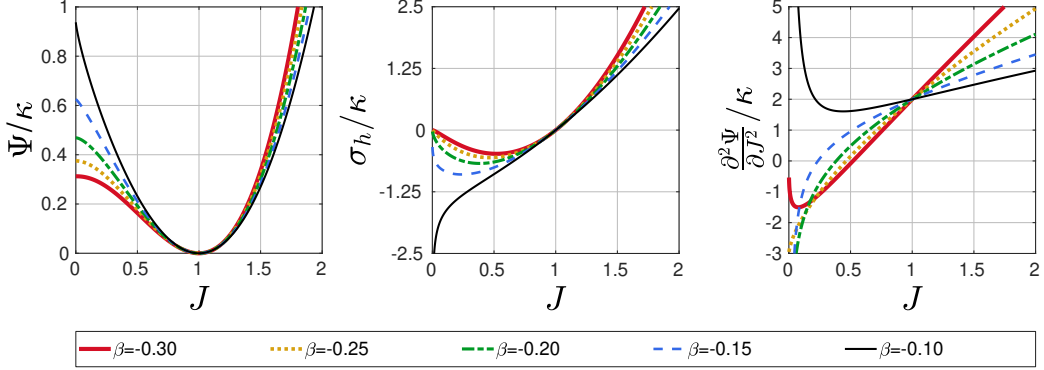


Figure 4: The normalized strain energy density (left), hydrostatic stress (middle), and tangent modulus (right), for the hyperfoam formulation. Curves drawn for $J = [0, 2]$, $\mu = 1$, $\alpha = 8$, and $\beta = [-0.3, -0.1]$

222 The illustrated behaviour for the domain $-\frac{1}{3} < \beta < 0$ when $\alpha > 0$ would
 223 lead one to add the constraint $\beta > 0$ for this formulation. Figure 5 explores
 224 the effect of varying α when $\beta > 0$. In terms of the tangent modulus it may
 225 be seen to decay, become constant, or become negative. The hydrostatic
 226 stress for $\alpha \leq 6$ is seen to reach a maximum and become constant or reduced
 227 with increasing J (due to negative stiffness). It was found that a negative
 228 tangent modulus may occur when $0 < \alpha \leq 6$ (see expansion domain for the
 229 graphs for $\alpha \leq 6$). Hence to avoid this it appears that $\alpha > 6$ is an additional
 230 constraint to avoid a negative tangent modulus if $\beta > 0$.

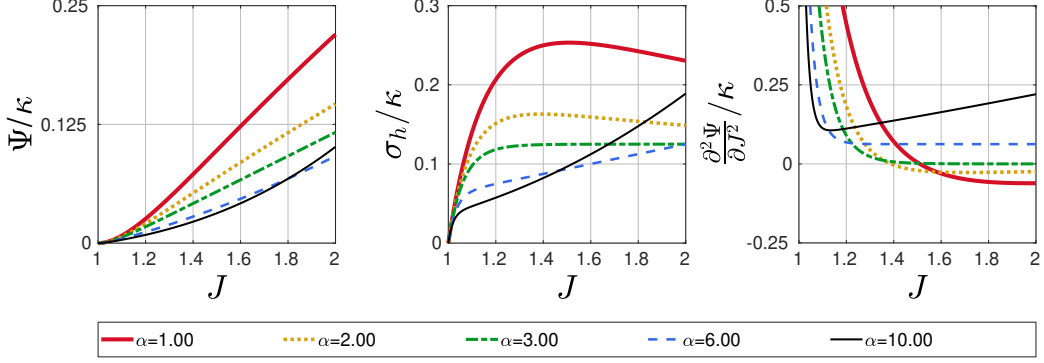


Figure 5: The normalized strain energy density (left), hydrostatic stress (middle), and tangent modulus (right), for the hyperfoam formulation. Curves drawn for $J = [1, 2]$, $\mu = 1$, $\beta = 5$, and $\alpha = [1, 10]$

231 Figure 6 presents the effect of varying β (when $\beta > 0$) when $\alpha > 6$
 232 ($\alpha = 8$). It is clear that a positive β value enhances the shrinkage domain
 233 while suppressing the expansion domain.

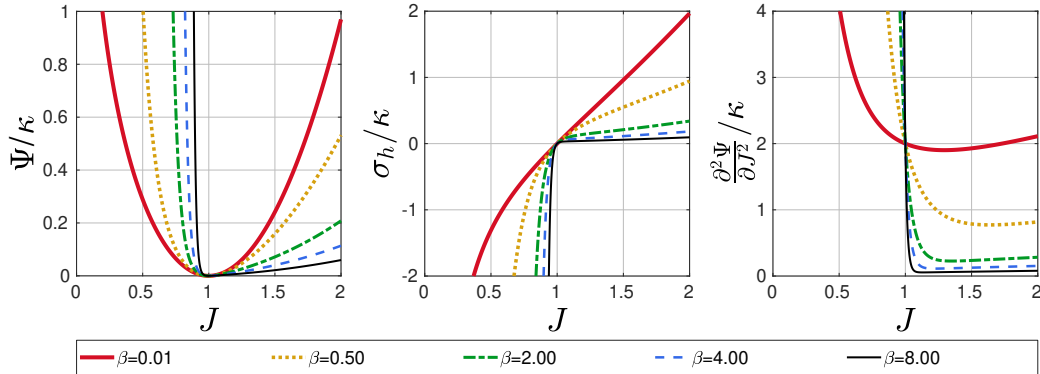


Figure 6: The normalized strain energy density (left), hydrostatic stress (middle), and tangent modulus (right), for the hyperfoam formulation. Curves drawn for $J = [0, 2]$, $\mu = 1$, $\alpha = 8$, and $\beta = [0.01, 8]$

234 Figure 7 is similar to Figure 6 except now a negative α is explored ($\alpha =$
 235 -8). These graphs show that now β changes its role to instead enhance the
 236 expansion domain while suppressing the shrinkage domain. Furthermore, it
 237 was observed that a negative tangent modulus may occur if β is close to zero
 238 (see graph for $\beta = 0.01$).

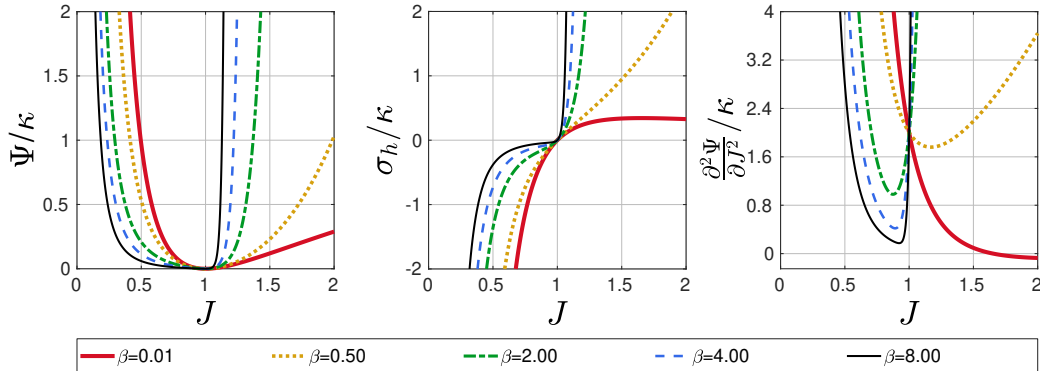


Figure 7: The normalized strain energy density (left), hydrostatic stress (middle), and tangent modulus (right), for the hyperfoam formulation. Curves drawn for $J = [0, 2]$, $\mu = 1$, $\alpha = -8$, and $\beta = [0.01, 8]$

239 In summary, in the above analysis, several additional constraints have
 240 been identified for the hyperfoam formulation. It appears $\beta > 0$ is a con-
 241 straint. In addition, if a positive α parameter is used, $\alpha > 6$ appears a
 242 requirement. If instead negative α values are employed a negative tangent
 243 modulus might occur for β values close to 0. It is therefore concluded that
 244 the hyperfoam formulation is highly constrained in terms of the choice of β
 245 and α .

246 For conventional Ogden hyperelastic formulations (see [35]) the param-
 247 eter α usually controls the degree of non-linearity (or strain hardening) pre-
 248 dominantly for the deviatoric behaviour, and for fitting, positive or nega-
 249 tive α parameters may required. However, as demonstrated here, for this
 250 Ogden-like hyperfoam formulation, α not only strongly influences the vol-
 251 umetric behaviour, it also changes the role of β (from enhancing shrinkage
 252 to enhancing expansion) when it changes sign. Furthermore, the suggested
 253 constraint $\alpha > 6$ (for $\alpha > 0$) may impose a potentially undesirable degree
 254 of non-linearity on the deviatoric response. For instance, some materials
 255 may demonstrate little strain stiffening such that they require $\alpha < 6$ (this
 256 includes Neo-Hookean behaviour, which requires $\alpha = 2$). Finally, even if
 257 suitable constraints are implemented, this formulation does not offer inde-
 258 pendent control in terms of enhancement for the shrinkage and expansion
 259 domains, it therefore does not satisfy criteria X of Table 1.

260 *3.5. The Doll and Schweizerhof [10] formulation*

261 Doll and Schweizerhof [10] proposed the following volumetric strain en-
 262 ergy density formulation:

$$\Psi(J) = \frac{\kappa}{\alpha + \beta} \left(\frac{1}{\alpha + 1} J^{\alpha+1} + \frac{1}{\beta - 1} J^{-(\beta-1)} \right) - \frac{\kappa}{(\alpha + 1)(\beta - 1)} \quad (16)$$

263 with the material parameter constraints: $\alpha > 0$ and $\beta > 1$. Besides satisfying
 264 all criteria listed in Table 1, this formulation also offers some control over
 265 the response in shrinkage and expansion. Furthermore, by choosing $\alpha = \beta$
 266 the pressure symmetry $p(J) = -p(\frac{1}{J})$ is obtained, and by using $\beta = \alpha + 2$
 267 one obtains symmetry in terms of strain energy, i.e. $\Psi(J) = \Psi(\frac{1}{J})$. Figure
 268 8 illustrates the effect of the parameter α . It enhances the response for
 269 expansion while mildly suppressing the response in expansion.

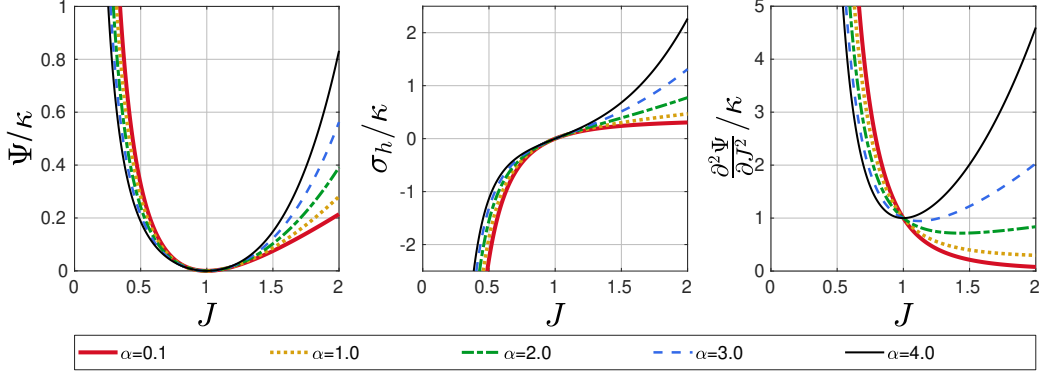


Figure 8: The normalized strain energy density (left), hydrostatic stress (middle), and tangent modulus (right), for the Doll and Schweizerhof [10] formulation. Curves drawn for $J = [0, 2]$, $\kappa = 1$, $\beta = 3$, and $\alpha = [0.1, 5]$

270 The parameter β has the opposite effect, as Figure 9 shows, since it
 271 enhances the response for shrinkage while suppressing the response in expan-
 272 sion.

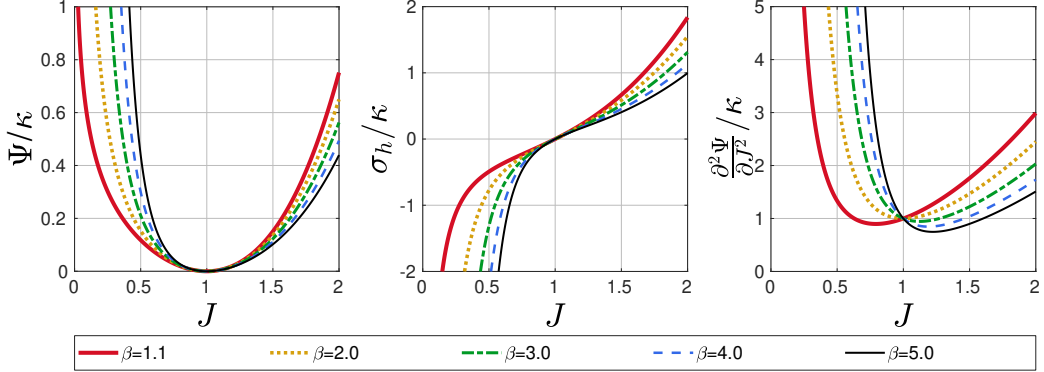


Figure 9: The normalized strain energy density (left), hydrostatic stress (middle), and tangent modulus (right), for the Doll and Schweizerhof [10] formulation. Curves drawn for $J = [0, 2]$, $\kappa = 1$, $\alpha = 3$, and $\beta = [1.1, 5]$

273 Although this formulation offers a way to control the response for shrink-
 274 age and expansion through the parameters α and β , both parameters have
 275 an effect on both domains. Therefore, since the control is not independent,
 276 criteria X of Table 1 is not fully met.

277 Furthermore, it is noted here that this formulation has the property that
 278 the minimum stiffness state need not be at $J = 1$ (see location of minima in

²⁷⁹ the image on the right of Figure 9). Although this is in principle not invalid,
²⁸⁰ it may not be realistic or desirable.

²⁸¹ 4. The proposed volumetric strain energy density formulations

²⁸² Three novel volumetric strain energy densities are presented in this section
²⁸³ which offer separate control over the strain dependent behaviour for shrinkage
²⁸⁴ and expansion.

²⁸⁵ 4.1. Formulation 1

²⁸⁶ The first formulation is inspired by equation 6. A power was added to
²⁸⁷ the volume ratio to enable control of the degree of strain stiffening. Next
²⁸⁸ two terms were created such that one features a positive power and one a
²⁸⁹ negative power, the former being most sensitive to expansion while the latter
²⁹⁰ is most sensitive to shrinkage, leading to:

$$\Psi_{vol}(J) = \frac{\kappa}{4} \left(\frac{1}{\beta_1^2} (J^{\beta_1} - 1)^2 + \frac{1}{\beta_2^2} (J^{-\beta_2} - 1)^2 \right) \quad (17)$$

²⁹¹ Besides the bulk modulus κ , this formulation features the material param-
²⁹² eters β_1 and β_2 , which control the degree of strain stiffening in terms of
²⁹³ expansion and shrinkage respectively, with $\kappa \in \mathbb{R}_{>0}$, $\beta_1 \in \mathbb{R}_{>2}$, and $\beta_2 \in \mathbb{R}_{>0}$.

²⁹⁴ The hydrostatic stress for this formulation is:

$$\sigma_h(J) = \frac{\kappa}{2J} \left(\frac{1}{\beta_1} (J^{2\beta_1} - J^{\beta_1}) - \frac{1}{\beta_2} (J^{-2\beta_2} - J^{-\beta_2}) \right) \quad (18)$$

²⁹⁵ and the tangent modulus:

$$\begin{aligned} \frac{\partial^2 \Psi_{vol}(J)}{\partial J^2} &= \frac{\kappa}{2J^2} \left[\left((2 - \frac{1}{\beta_1}) J^{2\beta_1} - (1 - \frac{1}{\beta_1}) J^{\beta_1} \right) \right. \\ &\quad \left. + \left((2 + \frac{1}{\beta_2}) J^{-2\beta_2} - (1 + \frac{1}{\beta_2}) J^{-\beta_2} \right) \right] \end{aligned} \quad (19)$$

²⁹⁶ Figure 10 schematically illustrates the effect of the parameters κ , β_1 , and
²⁹⁷ β_2 , on the hydrostatic stress.

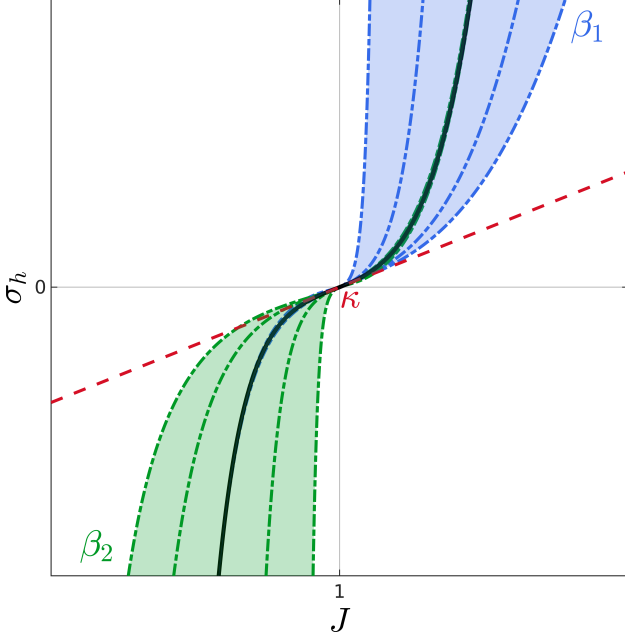


Figure 10: A schematic illustration of a typical σ_h curve illustrating the nature of the parameters κ , the bulk modulus setting the initial slope, β_1 , setting the rate of strain stiffening in expansion, β_2 , setting the rate of strain stiffening in shrinkage.

298

Figure 11 shows the effect of varying the bulk modulus κ .

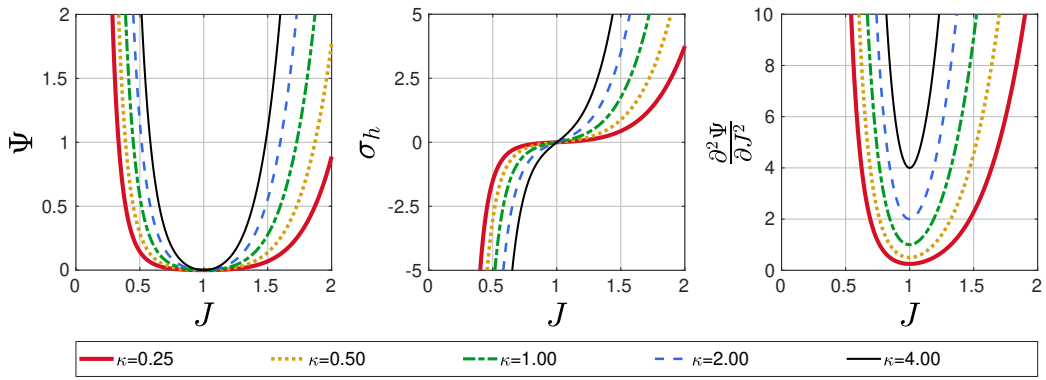


Figure 11: The effect of κ . The strain energy density (left), hydrostatic stress (middle), and tangent modulus (right) for formulation 1. Curves drawn for $J = [0, 2]$, $\beta_1 = 4$, $\beta_2 = 2$, $\kappa = [0.25, 4]$.

299

Figure 12 and 13 illustrate the effect of varying β_1 and β_2 respectively,

300 demonstrating near independent control of strain hardening for the expansion
 301 and shrinkage domains.

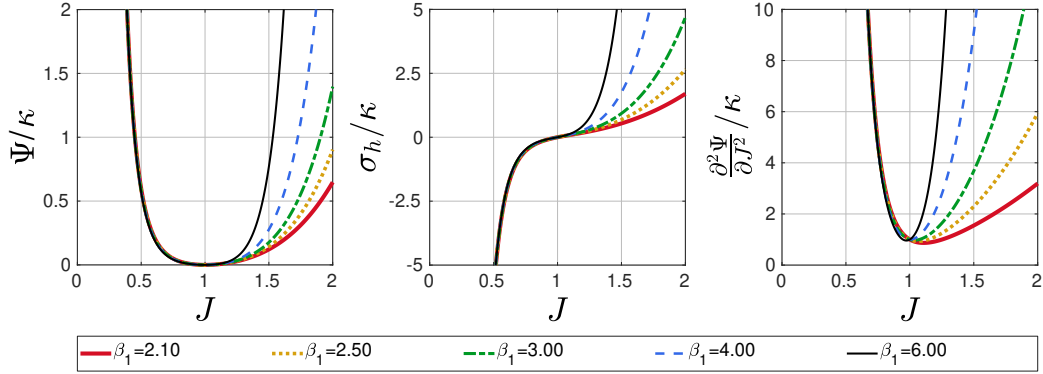


Figure 12: The effect of β_1 . The normalized strain energy density (left), hydrostatic stress (middle), and tangent modulus (right) for formulation 1. Curves drawn for $J = [0, 2]$, $\kappa = 1$, $\beta_2 = 2$, $\beta_1 = [2.1, 6]$.

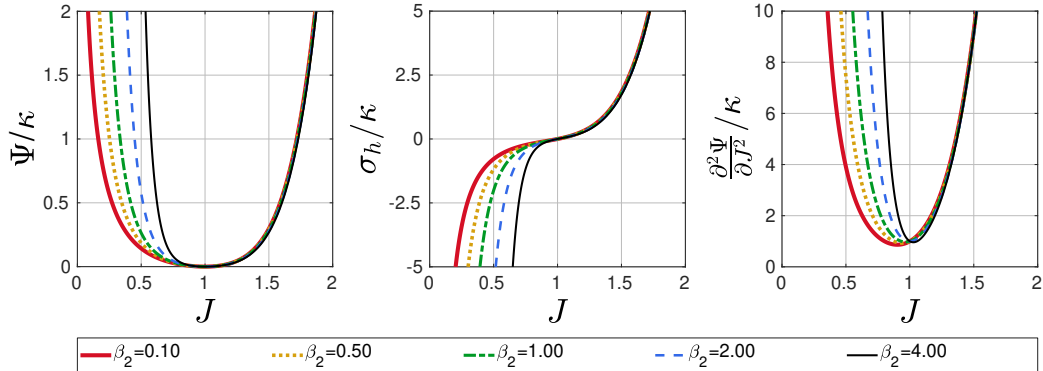


Figure 13: The effect of β_2 . The normalized strain energy density (left), hydrostatic stress (middle), and tangent modulus (right) for formulation 1. Curves drawn for $J = [0, 2]$, $\kappa = 1$, $\beta_1 = 2$, $\beta_2 = [0.1, 4]$.

302 Although near independent control is seen for both the magnitude and
 303 degree of strain stiffening of the responses for shrinkage and expansion, it is
 304 noted here that, similar to the Doll and Schweizerhof [10] formulation, the
 305 minimum stiffness is not guaranteed to be κ and may not be found at $J = 1$
 306 (Note the shift in the minima for the tangent modulus in Figures 12 and 13).
 307 Formulation 2, discussed in the next section, avoids this behaviour.

308 In Appendix A two variations of the above formulation are briefly ex-
 309 plored. In equation A.1 of Appendix A.1 a weighting factor was introduced
 310 with the aim of providing further control over the dominance of the expan-
 311 sion and shrinkage terms. However, this change results in a possible negative
 312 tangent modulus for particular parameter choices.

313 To address the fact that the minimum stiffness of formulation 1 only
 314 lies at $J = 1$ if $\beta_2 = \beta_1 + 2$, equation A.4 of Appendix A.2 describes a
 315 switch statement based decoupling of the expansion and shrinkage terms
 316 such that the expansion term is used if $J \geq 1$, and the shrinkage term if
 317 $J < 1$. Although this alternative form forces the minimum tangent modulus
 318 to occur at $J = 1$, and satisfies all constraints listed in Table 1, it presents
 319 with a non-smooth stiffness at $J = 1$, which may not be desirable.

320 *4.2. Formulation 2*

321 This section discusses a formulation which was inspired by the inverse
 322 sigmoid shape of the hydrostatic stress. A tangent function was chosen here
 323 since it presents with a rather elegant integral and derivative. The strain
 324 energy density for the proposed form is:

$$\Psi_{vol}(J) = -\kappa a^2 \ln \left(\cos \left(\frac{J-1}{a} \right) \right) \quad (20)$$

325 The derivative with J provides the hydrostatic stress:

$$\sigma_h(J) = \kappa a \tan \left(\frac{J-1}{a} \right) \quad (21)$$

326 The second derivative provides the tangent modulus:

$$\frac{\partial^2 \Psi_{vol}(J)}{\partial J^2} = \kappa \sec^2 \left(\frac{J-1}{a} \right) \quad (22)$$

327 The parameter a is defined as:

$$a = \frac{2}{\pi} \begin{cases} J_1 - 1 & J \geq 1 \\ J_2 - 1 & J < 1 \end{cases} \quad (23)$$

328 This formulation features three material parameters, the bulk modulus κ and
 329 two volume ratio parameters defining "lock-up" stretches, J_1 (with $J_1 > 1$),

330 and J_2 (with $0 \leq J_2 < 1$). Figure 14 contains a schematic illustration of the
 331 nature of these parameters in relation to the hydrostatic stress.

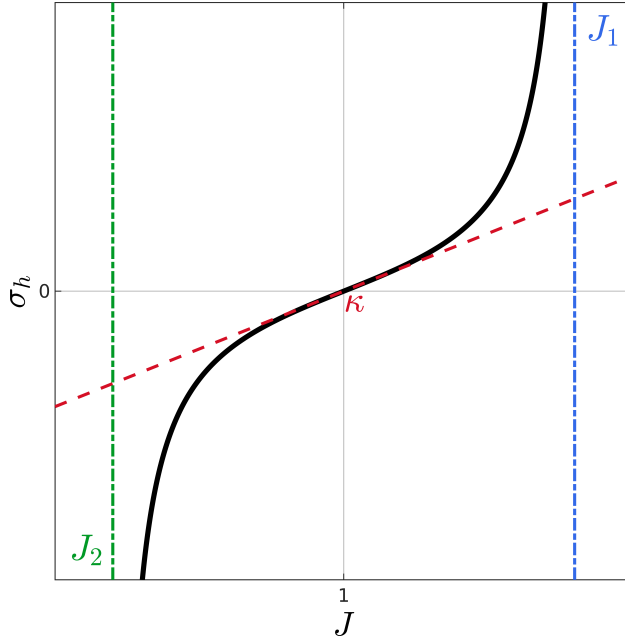


Figure 14: A schematic illustration of a typical σ_h curve illustrating the nature of the parameters κ , the bulk modulus setting the initial slope, J_1 , setting the maximum volume ratio asymptote, and J_2 , setting a minimum volume ratio asymptote.

332 Both J_1 and J_2 define a volume ratio at which an asymptote exists for
 333 strain energy, hydrostatic stress, and the tangent modulus. Numerical im-
 334 plementations therefore should feature the constraints:

$$\begin{aligned} \Psi_{vol}(J \geq J_1) &= \Psi_{vol}(J \leq J_2) = \infty \\ p(J \geq J_1) &= -p(J \leq J_2) = \infty \end{aligned} \tag{24}$$

$$\frac{\partial^2 \Psi_{vol}(J \geq J_1)}{\partial J^2} = \frac{\partial^2 \Psi_{vol}(J \leq J_2)}{\partial J^2} = \infty$$

335 The bulk modulus κ sets the slope for the hydrostatic stress at $J = 1$.
 336 Beyond $J = 1$ the volume ratios J_1 and J_2 determine how rapidly stiffness
 337 is enhanced for the expansion and shrinkage domains. If a material exhibits
 338 a behaviour such that further volume change beyond a particular point is
 339 hindered, this can be modelled using an appropriate choice for these volume

340 ratio asymptote levels. For many materials however $J_2 = 0$ is most appropriate
 341 as this is where this asymptote may naturally lie. Clearly if $J_2 = 0$ is
 342 kept fixed this formulation has only the two remaining parameters κ and J_1 .
 343 Both asymptote levels can be set at a level beyond the expected deformation
 344 levels or brought in closer to further enhance strain stiffening. Figure 15
 345 illustrates the effect of varying the bulk modulus κ and demonstrates how it
 346 changes the slope at $J = 1$ for the hydrostatic stress.

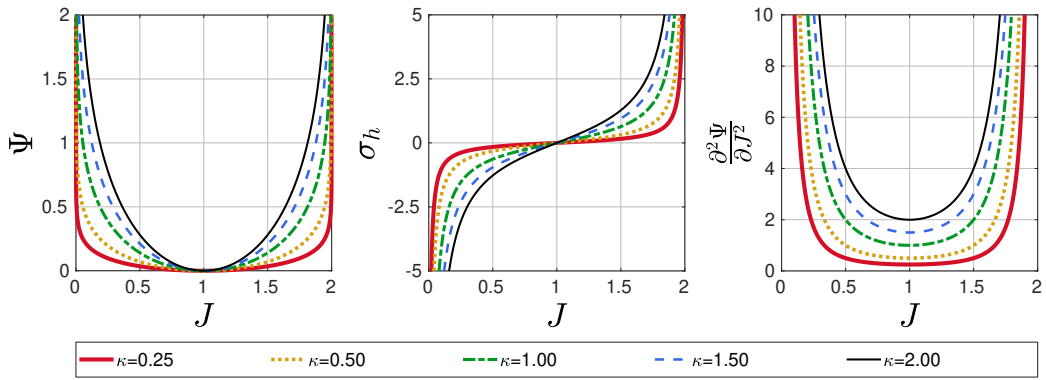


Figure 15: The effect of the bulk modulus. The normalized strain energy density (left), hydrostatic stress (middle), and tangent modulus (right) for formulation 2. Curves drawn for $J = [0, 2]$, $J_2 = 0$, $J_1 = 2$ and $\kappa = [0.25, 2]$

347 Figure 16 presents the effect of varying J_1 . The parameter J_1 is seen to
 348 shift the location of the asymptote in the expansion domain.

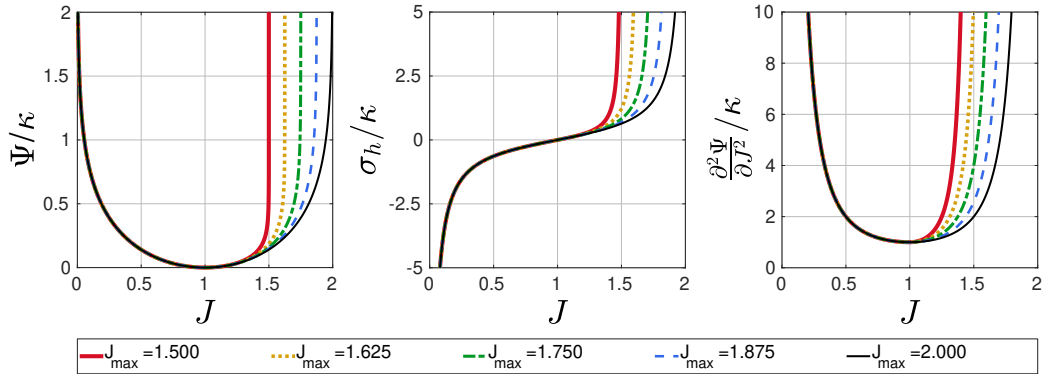


Figure 16: The effect of the J_1 . The normalized strain energy density (left), hydrostatic stress (middle), and tangent modulus (right) for formulation 2. Curves drawn for $\kappa = 1$, $J = [0, 2]$, $J_2 = 0$ and $J_1 = [1.5, 2]$

349 Figure 17 presents the effect of varying J_2 . It is clear how J_2 enables one
 350 to alter the location of the asymptote in the shrinkage domain.

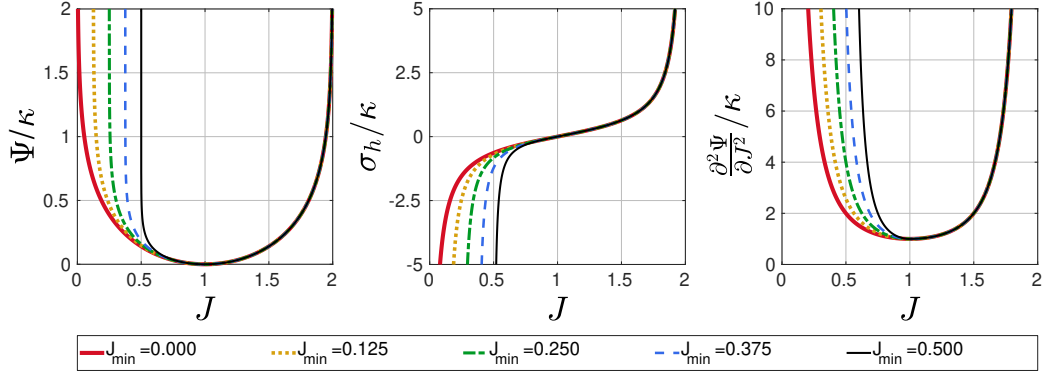


Figure 17: The effect of the J_2 . The normalized strain energy density (left), hydrostatic stress (middle), and tangent modulus (right) for formulation 2. Curves drawn for $\kappa = 1$, $J = [0, 2]$, $J_1 = 2$ and $J_2 = [0, 0.5]$

351 From Figures 15, 17, and 16 it is clear that, contrary to the other formu-
 352 lations, the minimum tangent modulus is guaranteed to occur at $J = 1$ and
 353 is equal to κ .

354 Furthermore, one may note that the following simultaneous symmetries
 355 exist:

$$\Psi_{vol}(J_s) = \Psi_{vol}(J_e), \quad \sigma_h(J_s) = -\sigma_h(J_e), \quad \frac{\partial^2 \Psi_{vol}(J_s)}{\partial J^2} = \frac{\partial^2 \Psi_{vol}(J_e)}{\partial J^2} \quad (25)$$

356 (where subscript s and e refer to shrinkage and expansion respectively), if

$$J_e = (J_s - 1) \frac{J_1 - 1}{J_2 - 1} + 1, \quad J_s = (J_e - 1) \frac{J_2 - 1}{J_1 - 1} + 1 \quad (26)$$

357 Therefore if simultaneous symmetry in terms of J and $1/J$ is desired one
 358 could use:

$$J_2 = \frac{1}{J_1} \quad (27)$$

359 Formulation 2 adheres to all criteria of Table 1, with the exception of
 360 criteria *VII* and *VIII*, due to the existence of the asymptote at J_1 in the ex-
 361 pansion domain. Indeed it may be deemed unnatural to have the asymptote
 362 depart from $J = 0$ for the shrinkage domain, or to have an asymptote at all

for the expansion domain. Appendix A.3 therefore presents a variation to formulation 2 which does not have these features, instead it employs a form similar to equation 7 but with natural asymptotic behaviour added at $J = 0$.

4.3. Formulation 3

Formulation 3, proposed below, is an extension of formulation 2, of Section 4.2, to capture non-monotonic strain stiffening, as observed in cellular materials, lattices, and foams [60, 5]. As illustrated in Figure 18, such materials exhibit three main phases during large volumetric compression [60]: I) an initial linear or moderately strain stiffening phase; II) a reduced stiffness/plateau region due to elastic buckling of the material microstructure; and III) a region of increased stiffness due to densification of the structure. Such non-monotonic stiffening behaviour with an elastic buckling plateau region is observed for elastometric foams, such as polyurethane foams (e.g. [13, 17]), and cork (e.g. [61, 5, 62, 47, 5]).

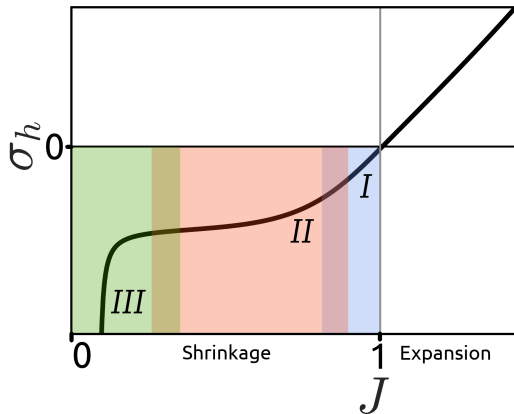


Figure 18: The typical response of a cellular solid to shrinkage and expansion. The shrinkage domain typically features several phases, e.g. an initial elastic domain (I), followed by a compaction domain (II), and a densification domain (III).

As seen in Section 4.2, Formulation 2 features the \tan function creating a vertical sigmoid shape for the hydrostatic stress. In order to expand formulation 2 to allow for a reduced stiffness/plateau region, an additional horizontal sigmoid function is added; in this case a \tanh function is used, with asymptotes parallel to the J axis. Conveniently these functions share conceptually similar integrals and derivatives. We propose the following strain energy

³⁸³ density function:

$$\Psi_{vol}(J) = \kappa \left[-(1-q)a^2 \ln(\cos\left(\frac{J-1}{a}\right)) + qb^2 \ln(\cosh\left(\frac{J-1}{b}\right)) \right] \quad (28)$$

³⁸⁴ resulting in the following expression for hydrostatic stress:

$$\sigma_h(J) = \kappa \left[(1-q)a \tan\left(\frac{J-1}{a}\right) + qb \tanh\left(\frac{J-1}{b}\right) \right] \quad (29)$$

³⁸⁵ with the following expression for tangent modulus:

$$\frac{\partial^2 \Psi_{vol}(J)}{\partial J^2} = \kappa \left[(1-q) \sec^2\left(\frac{J-1}{a}\right) + q \operatorname{sech}^2\left(\frac{J-1}{b}\right) \right] \quad (30)$$

³⁸⁶ The parameters a , b , and q are defined as:

$$a = \frac{2}{\pi} \begin{cases} J_1 - 1 & J \geq 1 \\ J_2 - 1 & J < 1 \end{cases} \quad b = \frac{1}{\kappa} \begin{cases} s_1 & J \geq 1 \\ s_2 & J < 1 \end{cases} \quad q = \begin{cases} q = q_1 & J \geq 1 \\ q = q_2 & J < 1 \end{cases} \quad (31)$$

³⁸⁷ In all cases independent values can be specified for shrinkage ($J < 1$) and
³⁸⁸ expansion ($J > 1$). The parameter a is the same as for formulation 2 where
³⁸⁹ J_2 and J_1 set the volume ratios for the two vertical asymptotes. Parameters
³⁹⁰ s_2 and s_1 set the hydrostatic stress asymptotes of the horizontal sigmoid
³⁹¹ function (\tanh) in expansion and shrinkage, respectively. The parameters
³⁹² q_1 and q_2 set the relative contributions of the monotonic strain stiffening
³⁹³ behaviour of the \tan component and the hydrostatic stress plateau behaviour
³⁹⁴ of the \tanh component. If $q_i = 0$ formulation 2 is recovered, with monotonic
³⁹⁵ strain stiffening. Conversely, if $q_i = 1$ a plateau in hydrostatic stress is
³⁹⁶ obtained, but this is not followed by a high stiffness densification region.
³⁹⁷ Figure 19 is a schematic illustration to highlight the effect of the material
³⁹⁸ parameters on the hydrostatic stress. The six physically based parameters
³⁹⁹ can be used to precisely specify the three phases of volumetric deformation
⁴⁰⁰ described above.

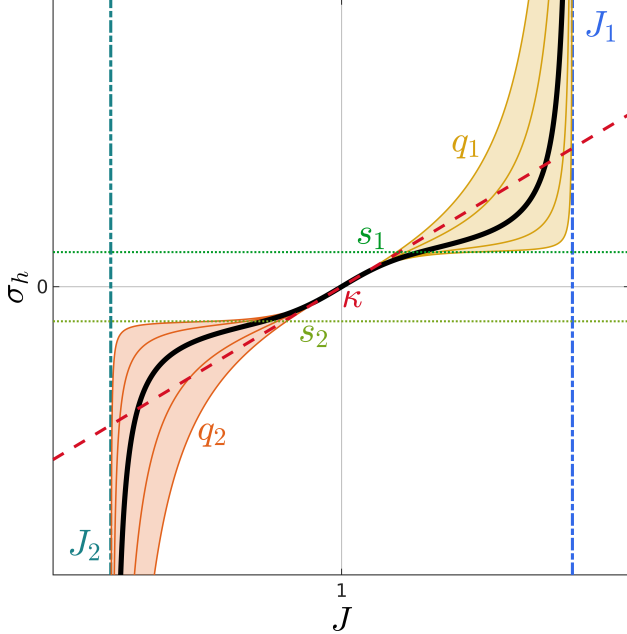


Figure 19: A schematic illustration of a typical σ_h curve illustrating the nature of the parameters κ , the bulk modulus setting the initial slope, J_1 , setting the maximum volume ratio asymptote, and J_2 , setting a minimum volume ratio asymptote, s_1 , setting the softening stress in expansion, q_1 setting the dominance of the softening in expansion, s_2 , setting the softening stress in shrinkage, and q_2 setting the dominance of the softening in shrinkage.

401 We next provide a parametric investigation of the effect of varying the
 402 parameters s_1 , s_2 , q_1 , and q_2 . The effect of κ , J_1 and J_2 is equivalent to
 403 that of formulation 2 (see Figure 15, 17, and 16 respectively) and therefore
 404 not repeated graphically here. Figure 20 shows the effect of varying s_1 .
 405 This parameter sets the plateau stress level for expansion for the horizontal
 406 sigmoid function.

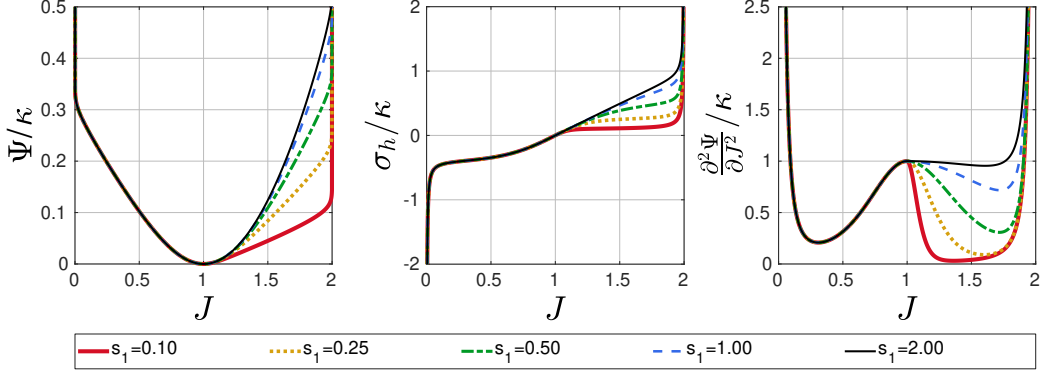


Figure 20: The effect of the s_1 . The normalized strain energy density (left), hydrostatic stress (middle), and tangent modulus (right) for formulation 3. Curves drawn for $\kappa = 1$, $J = [0, 2]$, $J_1 = 2$, $J_2 = 0$, $q_1 = 0.98$, $q_2 = 0.98$, $s_1 = [0.1, 2]$, $s_2 = 0.4$

407 Figure 21 shows the effect of varying s_2 . This parameter sets the plateau
 408 stress level for shrinkage for the horizontal sigmoid function (note that al-
 409 though the hydrostatic stress is negative during shrinkage, s_2 is here defined
 410 as a positive number).

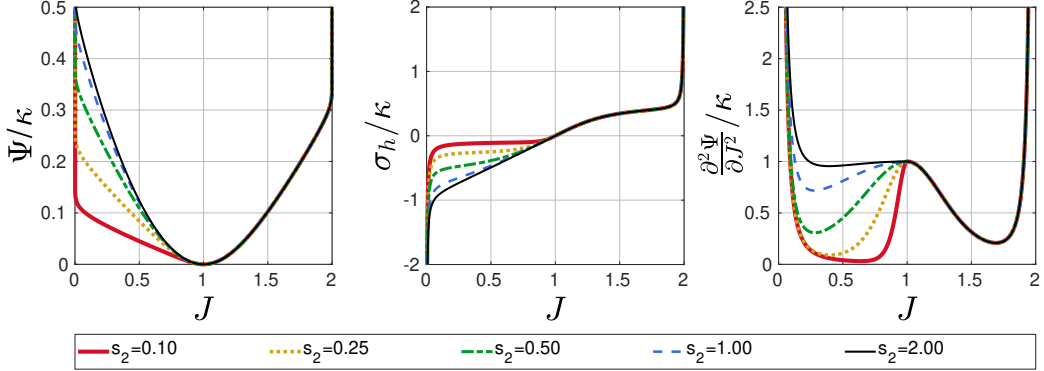


Figure 21: The effect of the s_2 . The normalized strain energy density (left), hydrostatic stress (middle), and tangent modulus (right) for formulation 3. Curves drawn for $\kappa = 1$, $J = [0, 2]$, $J_1 = 2$, $J_2 = 0$, $q_1 = 0.98$, $q_2 = 0.98$, $s_1 = 0.4$, $s_2 = [0.1, 2]$

411 Figure 22 presents the effect of varying q_1 , which controls the dominance
 412 of the stiffness reduction/plateau behaviour in the expansion domain.

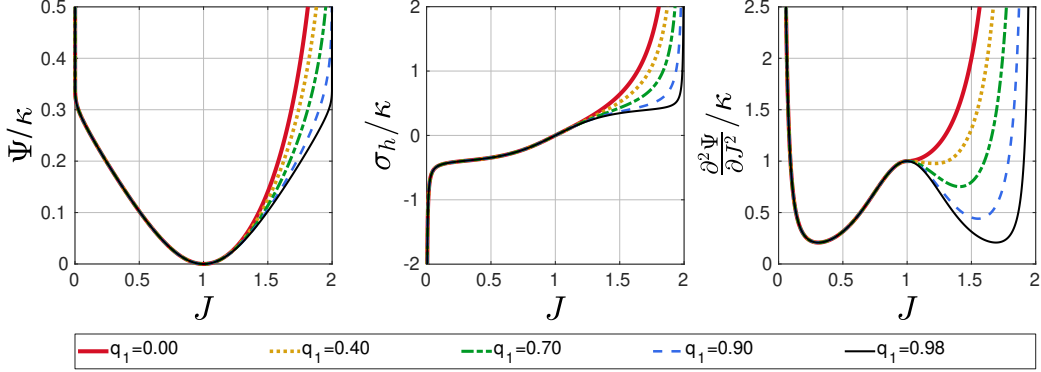


Figure 22: The effect of the q_1 . The normalized strain energy density (left), hydrostatic stress (middle), and tangent modulus (right) for formulation 3. Curves drawn for $\kappa = 1$, $J = [0, 2]$, $J_1 = 2$, $J_2 = 0$, $q_1 = [0, 0.98]$, $q_2 = 0.98$, $s_1 = 0.4$, $s_2 = 0.4$

413 Figure 23 presents the effect of varying q_2 , which controls the dominance
414 of the stiffness reduction/plateau behaviour in the shrinkage domain.

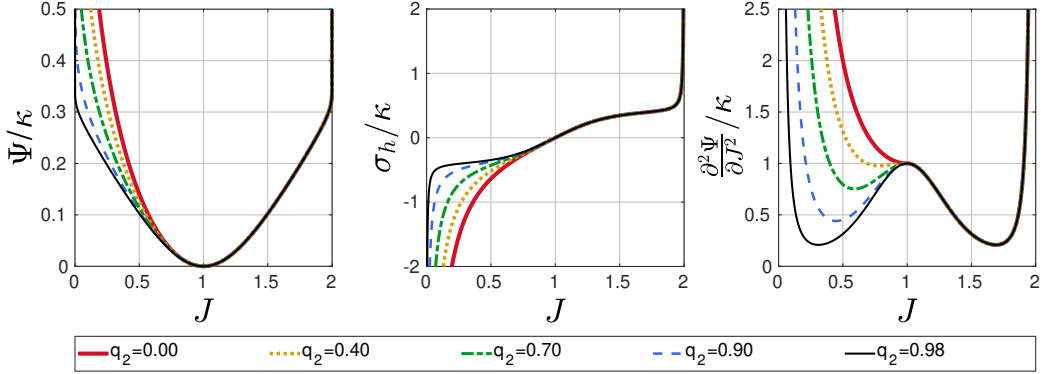


Figure 23: The effect of the q_2 . The normalized strain energy density (left), hydrostatic stress (middle), and tangent modulus (right) for formulation 3. Curves drawn for $\kappa = 1$, $J = [0, 2]$, $J_1 = 2$, $J_2 = 0$, $q_1 = 0.98$, $q_2 = [0, 0.98]$, $s_1 = 0.4$, $s_2 = 0.4$

415 4.4. Fitting to experimental data

416 To illustrate the ability of our new formulation 1-3 to capture experimen-
417 tal hydrostatic compression data, Figure 24 presents fits to data for neoprene
418 rubber foam [45] (1st column), flexible open-cell polyurethane cushioning
419 foam [17] (2nd column), natural cork [46] (3rd column), and rigid closed-
420 cell polyurethane foam [47] (4th column). As is evident from Figure 24, an

421 increasing amounts of stiffness reduction/plateau behaviour is observed in
 422 the experimental data (from left to right). In the case of the neoprene and
 423 open-cell foam the data represents fully elastic recoverable loading associ-
 424 ated with elastic buckling of the microstructure (rather than unrecoverable
 425 plastic buckling). Formulation 1 cannot accurately capture the non-linear
 426 monotonic strain stiffening behavior of neoprene rubber foam; the high stiff-
 427 ness behaviour at high volumetric strains is accurately predicted, but the
 428 stiffness at low volumetric strains is underpredicted. In contrast, formulation
 429 2 accurately predicts the neoprene rubber foam behaviour for the full range
 430 of experimental data. However, the inflection point observed for open-cell
 431 polyurethane cushioning foam and natural cork, and the plateau behaviour
 432 for closed-cell polyurethane foam are not captured. Formulation 3 is shown
 433 to accurately predict the reported experimental data for all four materials.

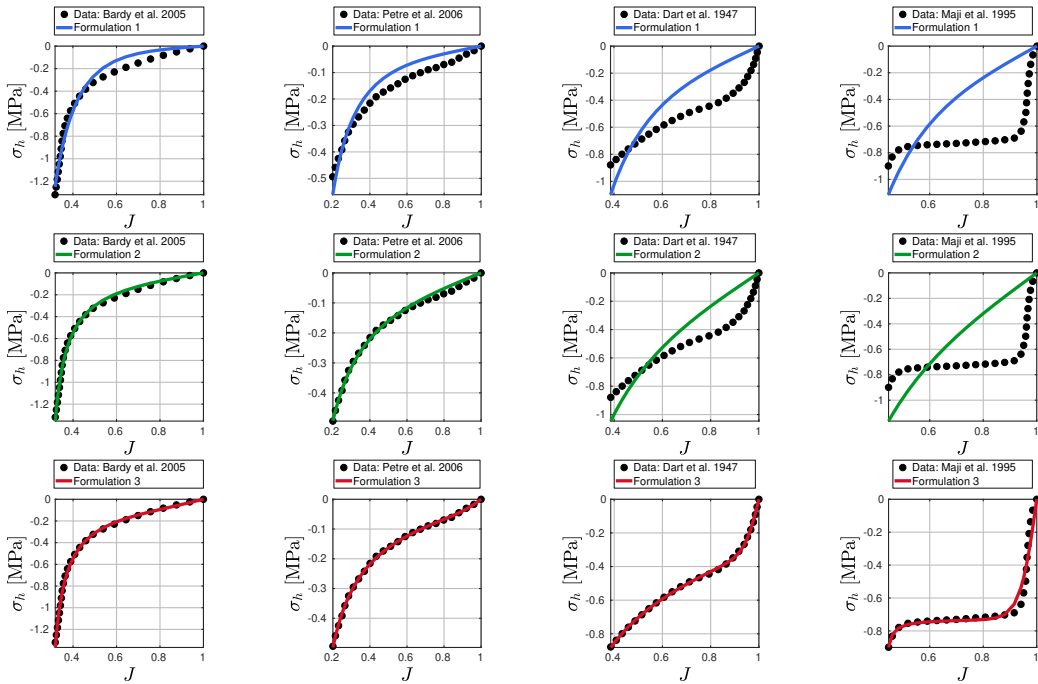


Figure 24: Fitting of formulation 1 (top row), formulation 2 (middle row), and formulation 3 (bottom row) to experimental hydrostatic compression data. From the left to the right the data was obtained from Bardy et al. [45], Petre et al. [17], Dart et al. [46], and , Maji et al. [47]

434 5. Discussion

435 Much attention has been given to the development of deviatoric strain en-
436 ergy density functions due to the traditional focus, of hyperelastic modelling,
437 on nearly-incompressible rubber materials (e.g. [33, 35, 34]), and assumed
438 incompressible soft tissue [6]. Comparatively few strain energy density func-
439 tions have been proposed for large volumetric deformations (e.g. [9, 7, 8, 10]).
440 We demonstrate here that well-established and commonly used volumetric
441 strain energy formulations are either not valid for large volumetric deforma-
442 tions, as they (i) do not adhere to criteria *I-IX* of Table 1, or (ii) do not
443 offer sufficient control, for either the shrinkage or the expansion domain, for
444 fitting of monotonic or non-monotonic strain stiffening behaviour (criteria *X*
445 of Table 1). Following a summary and critical analysis of common formu-
446 lations, and the pitfalls they exhibit, we propose three novel formulations
447 which uniquely: 1) are valid for large volumetric deformations, 2) offer sep-
448 arate control of the volumetric strain stiffening behaviour during shrinkage
449 (volume reduction) and expansion (volume increase), and 3) in the case of
450 formulation 3, offer the ability to capture non-monotonic volumetric stiff-
451 ening. The presented formulations offer superior flexibility for experimental
452 fitting of the large volumetric strain behaviour of hyperelastic materials, and
453 are demonstrated to adhere to all validity criteria listed in Table 1.

- 454 • Formulation 1 (Section 4.1) exhibits control of the magnitude and de-
455 gree of strain stiffening in shrinkage and expansion domains which is
456 not strongly coupled. This presents an incremental improvement of on
457 the model of Doll and Schweizerhof [10], in which the degree of strain
458 stiffening in shrinkage and expansion is strongly coupled. One property
459 of formulation 1 however is that the minimum of the tangent modulus
460 may not occur at $J = 1$, and is therefore lower than κ , for a particular
461 choice of parameters. Although this is a property shared with many
462 other formulations, and this does not render the formulation invalid by
463 any means, it may be deemed undesirable or unrealistic given particular
464 experimental data.
- 465 • Formulation 2 (Section 4.2) was developed to exhibit many of the prop-
466 erties of formulation 1 but also guarantees that the minimum stiffness
467 is found at $J = 1$. This model is formulated using logarithmic and
468 trigonometric functions, and features a bulk modulus κ to set the ini-
469 tial slope and two controllable asymptotes, one at the volume ratio

470 J_1 for expansion, and one at the volume ratio J_2 for shrinkage. For
471 shrinkage J_2 can be set at 0 to enable, for instance, infinite strain
472 energy at $J = 0$, as is common. However, it is possible to bring
473 J_2 closer to 1 to enable more rapid stiffening during volume reduction.
474 Similarly J_1 is the volume ratio at which an asymptote exists
475 for volume expansion. Control of strain stiffening in shrinkage and
476 expansion domains is fully decoupled, i.e. changes in one domain do
477 not influence the other. In terms of achieving symmetry, formulation
478 2 also enables, through an appropriate choice of parameters, simulta-
479 neous symmetry in terms of $\Psi_{vol}(J) = \Psi_{vol}(\frac{1}{J})$, $p(J) = -p(\frac{1}{J})$, and
480 $\partial^2\Psi_{vol}(J)/\partial J^2 = \partial^2\Psi_{vol}(\frac{1}{J})/\partial J^2$, i.e. the strain energy density, hy-
481 drostatic stress and tangent modulus for a given percentage volume
482 increase or decrease can be made to be equivalent. Furthermore, formu-
483 lation 2 ensures that, even for deviations from symmetry, the minimum
484 tangent modulus always occurs at $J = 1$ and is equal to κ . Appendix
485 A.3 provides a variation to formulation 2 whereby the asymptote pa-
486 rameters are avoided.

- 487 • Formulation 3 (Section 4.3) extends formulation 2, of Section 4.2, to
488 capture the non-monotonic stiffening reported for cellular materials,
489 lattices, and foams [60, 5]. A horizontal sigmoid function is superim-
490 posed on formulation 2 creating softening behaviour. The parameters
491 s_1 and s_2 define hydrostatic stress asymptotes on the horizontal sig-
492 moid function for the expansion and shrinkage domain respectively.
493 Furthermore parameters q_1 or q_2 define the dominance of these poten-
494 tial softening plateaus. Similar to formulation 2, formulation 3 offers
495 independent control of the behaviour for the expansion and shrinkage
496 domains.

497 Formulation 3 is shown to provide accurate predictions of the non-linear
498 pressure volumetric relationship under hydrostatic compression for four ma-
499 terials, namely: neoprene rubber foam [45], flexible open-cell polyurethane
500 cushioning foam [17], natural cork [46], and rigid closed-cell polyurethane
501 foam [47]. As discussed above, the ability to accurately model non-monotonic
502 volumetric shrinkage and expansion will be important for the simulation and
503 design of next-generation lattice materials, including ultraporous sponges
504 [26] graphene foams aerogels (e.g [27, 28, 29, 30]) in which elastic recovery
505 from compressive strains of 90% have been reported [31]. Graphene aerogels

506 can also be 3D printed [63] allowing for the creation of highly elastic, de-
507 formable, and complex lattices structures. Formulation 3 can also be used
508 to simulate non-monotonic volumetric stiffening of compressible biological
509 materials, such as arteries [64], and the myocardium [65]. Formulation 3 can
510 also be extended to account for plastic buckling in the plateau region (as
511 observed for polypropylene foams [66], metallic foams [67], and trabecular
512 bone [68, 69].

513 **6. Acknowledgements**

514 This project was funded by a European Union Horizon 2020 Research
515 and Innovation Program, under grant agreement No. 777072.

516 **References**

- 517 [1] T. A. Schaedler, W. B. Carter, Architected Cellular Materials, Annual
518 Review of Materials Research 46 (2016) 187–210.
- 519 [2] Fleck N. A., Deshpande V. S., Ashby M. F., Micro-architected ma-
520 terials: past, present and future, Proceedings of the Royal Society A:
521 Mathematical, Physical and Engineering Sciences 466 (2010) 2495–2516.
- 522 [3] J. W. C. Dunlop, P. Fratzl, Multilevel architectures in natural materials,
523 Scripta Materialia 68 (2013) 8–12.
- 524 [4] Mihai L. Angela, Alayyash Khulud, Goriely Alain, Paws, pads and
525 plants: the enhanced elasticity of cell-filled load-bearing structures, Pro-
526 ceedings of the Royal Society A: Mathematical, Physical and Engineer-
527 ing Sciences 471 (2015) 20150107.
- 528 [5] L. J. Gibson, K. E. Easterling, M. F. Ashby, The structure and mech-
529 anics of cork, Proceedings of the Royal Society of London. A. Mathematical
530 and Physical Sciences 377 (1981) 99–117.
- 531 [6] G. Chagnon, M. Rebouah, D. Favier, Hyperelastic energy densities for
532 soft biological tissues: A review, Journal of Elasticity 120 (2015) 129–
533 160.
- 534 [7] J. E. Bischoff, E. M. Arruda, K. Grosh, A New Constitutive Model
535 for the Compressibility of Elastomers at Finite Deformations, Rubber
536 Chemistry and Technology 74 (2001) 541–559.
- 537 [8] B. Storåkers, On material representation and constitutive branching in
538 finite compressible elasticity, Journal of the Mechanics and Physics of
539 Solids 34 (1986) 125–145.
- 540 [9] R. W. Ogden, Large Deformation Isotropic Elasticity: On the Corre-
541 lation of Theory and Experiment for Compressible Rubberlike Solids,
542 Proceedings of the Royal Society A: Mathematical, Physical and Engi-
543 neering Sciences 328 (1972) 567–583.
- 544 [10] S. Doll, K. Schweizerhof, On the Development of Volumetric Strain
545 Energy Functions, Journal of Applied Mechanics 67 (2016) 17–21.

- 546 [11] N. J. Mills, C. Fitzgerald, A. Gilchrist, R. Verdejo, Polymer foams for
547 personal protection: cushions, shoes and helmets, Composites Science
548 and Technology 63 (2003) 2389–2400.
- 549 [12] L. Savonnet, X. Wang, S. Duprey, Finite element models of the thigh-
550 buttock complex for assessing static sitting discomfort and pressure
551 sore risk: a literature review, Computer Methods in Biomechanics and
552 Biomedical Engineering 21 (2018) 379–388.
- 553 [13] D. Y. Kim, J. H. Bang, C. A. Lee, H. Y. Kim, K. Y. Choi, B. G.
554 Lim, Numerical evaluation of time-dependent sagging for low density
555 polyurethane foams to apply the long-term driving comfort on the seat
556 cushion design, International Journal of Industrial Ergonomics 64 (2018)
557 178–187.
- 558 [14] C. Briody, B. Duignan, S. Jerrams, J. Tiernan, The implementation
559 of a visco-hyperelastic numerical material model for simulating the be-
560 haviour of polymer foam materials, Computational Materials Science
561 64 (2012) 47–51.
- 562 [15] L. P. Cohen, A. Gefen, Deep tissue loads in the seated buttocks on an
563 off-loading wheelchair cushion versus air-cell-based and foam cushions:
564 finite element studies, International Wound Journal 14 (2017) 1327–
565 1334.
- 566 [16] E. Palta, H. Fang, D. C. Weggel, Finite element analysis of the Advanced
567 Combat Helmet under various ballistic impacts, International Journal
568 of Impact Engineering 112 (2018) 125–143.
- 569 [17] M. T. Petre, A. Erdemir, P. R. Cavanagh, Determination of elastomeric
570 foam parameters for simulations of complex loading, Computer Methods
571 in Biomechanics and Biomedical Engineering 9 (2006) 231–242.
- 572 [18] R. L. Actis, L. B. Ventura, D. J. Lott, K. E. Smith, P. K. Commean,
573 M. K. Hastings, M. J. Mueller, Multi-plug insole design to reduce peak
574 plantar pressure on the diabetic foot during walking, Medical & Biolog-
575 ical Engineering & Computing 46 (2008) 363–371.
- 576 [19] A. Ghassemi, A. R. Mossayebi, N. Jamshidi, R. Naemi, M. T. Karimi,
577 Manufacturing and finite element assessment of a novel pressure reduc-

- 578 ing insole for Diabetic Neuropathic patients, *Australasian Physical &*
579 *Engineering Sciences in Medicine* 38 (2015) 63–70.
- 580 [20] B. C. M. Murray, X. An, S. S. Robinson, I. M. v. Meerbeek, K. W.
581 O'Brien, H. Zhao, R. F. Shepherd, Poroelastic Foams for Simple Fab-
582 rication of Complex Soft Robots, *Advanced Materials* 27 (2015) 6334–
583 6340.
- 584 [21] N. G. Cheng, A. Gopinath, L. Wang, K. Iagnemma, A. E. Hosoi, Ther-
585 mally Tunable, Self-Healing Composites for Soft Robotic Applications,
586 *Macromolecular Materials and Engineering* 299 (2014) 1279–1284.
- 587 [22] C. Schlagenhauf, D. Bauer, K. Chang, J. P. King, D. Moro, S. Coros,
588 N. Pollard, Control of Tendon-Driven Soft Foam Robot Hands, in:
589 2018 IEEE-RAS 18th International Conference on Humanoid Robots
590 (Humanoids), pp. 1–7.
- 591 [23] L. Somm, D. Hahn, N. Kumar, S. Coros, Expanding Foam as the Mate-
592 rial for Fabrication, Prototyping and Experimental Assessment of Low-
593 Cost Soft Robots With Embedded Sensing, *IEEE Robotics and Au-*
594 *tomation Letters* 4 (2019) 761–768.
- 595 [24] L. R. Meza, S. Das, J. R. Greer, Strong, lightweight, and recoverable
596 three-dimensional ceramic nanolattices, *Science* 345 (2014) 1322–1326.
- 597 [25] M. R. Islam, G. Tudry, R. Bucinell, L. Schadler, R. C. Picu, Stochastic
598 continuum model for mycelium-based bio-foam, *Materials & Design* 160
599 (2018) 549–556.
- 600 [26] M. Mader, V. Jrme, R. Freitag, S. Agarwal, A. Greiner, Ultraporous,
601 Compressible, Wettable Polylactide/Polycaprolactone Sponges for Tis-
602 sue Engineering, *Biomacromolecules* 19 (2018) 1663–1673.
- 603 [27] D. Pan, C. Wang, X. Wang, Graphene Foam: Hole-Flake Network
604 for Uniaxial Supercompression and Recovery Behavior, *ACS Nano* 12
605 (2018) 11491–11502.
- 606 [28] J. Shang, Q.-S. Yang, X. Liu, C. Wang, Compressive deformation mech-
607 ism of honeycomb-like graphene aerogels, *Carbon* 134 (2018) 398–410.

- 608 [29] Y. Wu, N. Yi, L. Huang, T. Zhang, S. Fang, H. Chang, N. Li, J. Oh, J. A.
609 Lee, M. Kozlov, A. C. Chipara, H. Terrones, P. Xiao, G. Long, Y. Huang,
610 F. Zhang, L. Zhang, X. Lepr, C. Haines, M. D. Lima, N. P. Lopez, L. P.
611 Rajukumar, A. L. Elias, S. Feng, S. J. Kim, N. T. Narayanan, P. M.
612 Ajayan, M. Terrones, A. Aliev, P. Chu, Z. Zhang, R. H. Baughman,
613 Y. Chen, Three-dimensionally bonded spongy graphene material with
614 super compressive elasticity and near-zero Poissons ratio, *Nature Communications* 6 (2015) 6141.
615
- 616 [30] S. Chandrasekaran, P. G. Campbell, T. F. Baumann, M. A. Worsley,
617 Carbon aerogel evolution: Allotrope, graphene-inspired, and 3d-printed
618 aerogels, *Journal of Materials Research* 32 (2017) 4166–4185.
- 619 [31] H. Hu, Z. Zhao, W. Wan, Y. Gogotsi, J. Qiu, Ultralight and Highly
620 Compressible Graphene Aerogels, *Advanced Materials* 25 (2013) 2219–
621 2223.
- 622 [32] V. Tutwiler, R. I. Litvinov, A. P. Lozhkin, A. D. Peshkova, T. Lebedeva,
623 F. I. Ataullakhhanov, K. L. Spiller, D. B. Cines, J. W. Weisel, Kinetics
624 and mechanics of clot contraction are governed by the molecular and
625 cellular composition of the blood, *Blood* 127 (2016) 149–159.
- 626 [33] R. S. Rivlin, D. W. Saunders, Large Elastic Deformations of Isotropic
627 Materials. VII. Experiments on the Deformation of Rubber, *Philosophical
628 Transactions of the Royal Society A: Mathematical, Physical and
629 Engineering Sciences* 243 (1951) 251–288.
- 630 [34] L. R. G. Treloar, H. G. Hopkins, R. S. Rivlin, J. M. Ball, The Mechanics
631 of Rubber Elasticity, *Proceedings of the Royal Society A: Mathematical,
632 Physical and Engineering Sciences* 351 (1976) 301–330.
- 633 [35] R. Ogden, Non-linear elastic deformations, Dover Publications Inc.,
634 1984.
- 635 [36] M. C. Boyce, E. M. Arruda, Constitutive Models of Rubber Elasticity:
636 A Review, *Rubber Chemistry and Technology* 73 (2000) 504–523.
- 637 [37] J. C. Simo, R. L. Taylor, Penalty function formulations for incompressible
638 nonlinear elastostatics, *Computer Methods in Applied Mechanics and
639 Engineering* 35 (1982) 107–118.

- 640 [38] J. a. Weiss, B. N. Maker, S. Govindjee, Finite element implementa-
641 tion of incompressible, transversely isotropic hyperelasticity, Computer
642 Methods in Applied Mechanics and Engineering 135 (1996) 107–128.
- 643 [39] R. Hill, Aspects of Invariance in Solid Mechanics, in: C.-S. Yih (Ed.),
644 Advances in Applied Mechanics, volume 18, Elsevier, 1979, pp. 1–75.
- 645 [40] P. J. Blatz, W. L. Ko, Application of Finite Elastic Theory to the Defor-
646 mation of Rubbery Materials, Transactions of the Society of Rheology
647 6 (1962) 223–252.
- 648 [41] F. A. O. Fernandes, R. T. Jardin, A. B. Pereira, R. J. Alves de Sousa,
649 Comparing the mechanical performance of synthetic and natural cellular
650 materials, Materials & Design 82 (2015) 335–341.
- 651 [42] Z. Liu, M. G. Scanlon, Modelling Indentation of Bread Crumb by Finite
652 Element Analysis, Biosystems Engineering 85 (2003) 477–484.
- 653 [43] M. Ju, S. Mezghani, H. Jmal, R. Dupuis, E. Aubry, Parameter Es-
654 timation of a Hyperelastic Constitutive Model for the Description of
655 Polyurethane Foam in Large Deformation, Cellular Polymers 32 (2013)
656 21–40.
- 657 [44] B. Fazekas, T. J. Goda, Determination of the hyper-viscoelastic model
658 parameters of open-cell polymer foams and rubber-like materials with
659 high accuracy, Materials & Design 156 (2018) 596–608.
- 660 [45] E. Bardy, J. Mollendorf, D. Pendergast, Thermal conductivity and com-
661 pressive strain of foam neoprene insulation under hydrostatic pressure,
662 Journal of Physics D: Applied Physics 38 (2005) 3832–3840.
- 663 [46] S. L. Dart, H. A. Robinson, E. Guth, Elastic Properties of Cork: III.
664 Hydrostatic and Ordinary LoadCompression Curves for Cork, Journal
665 of Applied Physics 18 (1947) 474–478.
- 666 [47] A. Maji, H. Schreyer, S. Donald, Q. Zuo, D. Satpathi, Mechanical Prop-
667 erties of Polyurethane-Foam Impact Limiters, Journal of Engineering
668 Mechanics 121 (1995) 528–540.
- 669 [48] G. Holzapfel, Nonlinear solid mechanics: A continuum approach for
670 engineering, John Wiley & Sons Ltd., 2000.

- 671 [49] C. O. Horgan, J. G. Murphy, On the volumetric part of strain-energy
672 functions used in the constitutive modeling of slightly compressible solid
673 rubbers, International Journal of Solids and Structures 46 (2009) 3078–
674 3085.
- 675 [50] W. Ehlers, G. Eipper, The simple tension problem at large volumetric
676 strains computed from finite hyperelastic material laws, Acta Mechanica
677 130 (1998) 17–27.
- 678 [51] K. M. Moerman, GIBBON: The Geometry and Image-Based Bioengi-
679 neering add-On, The Journal of Open Source Software 3 (2018) 506.
- 680 [52] K. Moerman, A. J. Nederveen, C. K. Simms, Image Based Model Con-
681 struction , Boundary Condition Specification and Inverse Fea Control :
682 a Basic Matlab Toolkit for Febio, Proceedings of the 11th International
683 Symposium, Computer Methods in Biomechanics and Biomedical Engi-
684 neering (2013) 7–8.
- 685 [53] H. Hencky, The elastic behavior of vulcanized rubber, Rubber Chem-
686 tistry and Technology 6 (1933) 217–224.
- 687 [54] T. Sussman, K.-J. Bathe, A finite element formulation for nonlinear
688 incompressible elastic and inelastic analysis, Computers & Structures
689 26 (1987) 357–409.
- 690 [55] J. C. Simo, A framework for finite strain elastoplasticity based on max-
691 imum plastic dissipation and the multiplicative decomposition: Part i.
692 continuum formulation, Computer Methods in Applied Mechanics and
693 Engineering 66 (1988) 199–219.
- 694 [56] S. A. Maas, B. J. Ellis, G. A. Ateshian, J. A. Weiss, FEBio: Finite
695 elements for biomechanics, Journal of Biomechanical Engineering 134
696 (2012) 011005–011005.
- 697 [57] E. M. Arruda, M. C. Boyce, A three-dimensional constitutive model
698 for the large stretch behavior of rubber elastic materials, Journal of the
699 Mechanics and Physics of Solids 41 (1993) 389–412.
- 700 [58] H. F. Enderle, H. G. Kilian, T. Vilgis, Irreversible deformation of macro-
701 molecular networks, Colloid and Polymer Science 262 (1984) 696–704.

- 702 [59] H. F. Enderle, H. G. Kilian, General deformation modes of a van der
703 Waals network, in: Permanent and Transient Networks, Progress in
704 Colloid & Polymer Science, Steinkopff, 1987, pp. 55–61.
- 705 [60] L. J. Gibson, Biomechanics of cellular solids, *Journal of Biomechanics*
706 38 (2005) 377–399.
- 707 [61] M. Fortes, J. Fernandes, I. Serralheiro, M. Rosa, Experimental Deter-
708 mination of Hydrostatic Compression versus Volume Change Curves for
709 Cellular Solids, *Journal of Testing and Evaluation* 17 (1989) 67.
- 710 [62] L. Le Barbenchon, J. Girardot, J.-B. Kopp, P. Viot, Multi-scale foam :
711 3d structure/compressive behaviour relationship of agglomerated cork,
712 *Materialia* 5 (2019) 100219.
- 713 [63] Q. Zhang, F. Zhang, S. P. Medarametla, H. Li, C. Zhou, D. Lin, 3d
714 Printing of Graphene Aerogels, *Small* 12 (2016) 1702–1708.
- 715 [64] D. R. Nolan, J. P. McGarry, On the Compressibility of Arterial Tissue,
716 *Annals of Biomedical Engineering* 44 (2016) 993–1007.
- 717 [65] E. McEvoy, G. A. Holzapfel, P. McGarry, Compressibility and
718 Anisotropy of the Ventricular Myocardium: Experimental Analysis and
719 Microstructural Modeling, *Journal of Biomechanical Engineering* 140
720 (2018) 081004–081004–10.
- 721 [66] P. Viot, Hydrostatic compression on polypropylene foam, *International*
722 *Journal of Impact Engineering* 36 (2009) 975–989.
- 723 [67] V. S. Deshpande, N. A. Fleck, Multi-axial yield behaviour of polymer
724 foams, *Acta Materialia* 49 (2001) 1859–1866.
- 725 [68] N. Kelly, J. P. McGarry, Experimental and numerical characterisation
726 of the elasto-plastic properties of bovine trabecular bone and a trabec-
727 ular bone analogue, *Journal of the Mechanical Behavior of Biomedical*
728 *Materials* 9 (2012) 184–197.
- 729 [69] N. Kelly, N. M. Harrison, P. McDonnell, J. P. McGarry, An experi-
730 mental and computational investigation of the post-yield behaviour of
731 trabecular bone during vertebral device subsidence, *Biomechanics and*
732 *Modeling in Mechanobiology* 12 (2013) 685–703.

733 **Appendix A. Alternative formulations**

734 *Appendix A.1. Formulation 1 with a weighting factor*

735 In this variation of formulation 1 of section 4.1 a weighting factor $q \in [0, 1]$
 736 is introduced with the aim of scaling the contributions for expansion and
 737 shrinkage. The strain energy density for this variation is:

$$\Psi_{vol}(J) = \frac{\kappa}{2} \left(\frac{q}{\beta_1^2} (J^{\beta_1} - 1)^2 + \frac{1-q}{\beta_2^2} (J^{-\beta_2} - 1)^2 \right) \quad (\text{A.1})$$

738 Leading to the following expression for the hydrostatic stress:

$$\sigma_h(J) = \frac{\kappa}{J} \left(\frac{q}{\beta_1} (J^{2\beta_1} - J^{\beta_1}) - \frac{1-q}{\beta_2} (J^{-2\beta_2} - J^{-\beta_2}) \right) \quad (\text{A.2})$$

739 and the tangent modulus:

$$\begin{aligned} \frac{\partial^2 \Psi_{vol}(J)}{\partial J^2} &= \frac{\kappa}{J^2} \left[\frac{q}{\beta_1} \left((2\beta_1 - 1)J^{2\beta_1} - (\beta_1 - 1)J^{\beta_1} \right) \right. \\ &\quad \left. + \frac{1-q}{\beta_2} \left((2\beta_2 + 1)J^{-2\beta_2} - (\beta_2 + 1)J^{-\beta_2} \right) \right] \end{aligned} \quad (\text{A.3})$$

740 It is noted that if $q = 1$ and $\beta_1 = 1$ this formulation reduces to the familiar
 741 form of equation 6. Furthermore, if $q = 0.5$ and $\beta_2 = \beta_1 + 2$ the symmetry
 742 $\Psi_{vol}(J) = \Psi_{vol}(\frac{1}{J})$ is obtained.

743 Figure A.25 illustrates the effect of varying q , and shows how it allows
 744 one to control the dominance of the expansion and shrinkage contributions.
 745 Hence for fitting purposes this formulation offers flexibility in terms of both
 746 the magnitude and the degree of strain stiffening of the response.

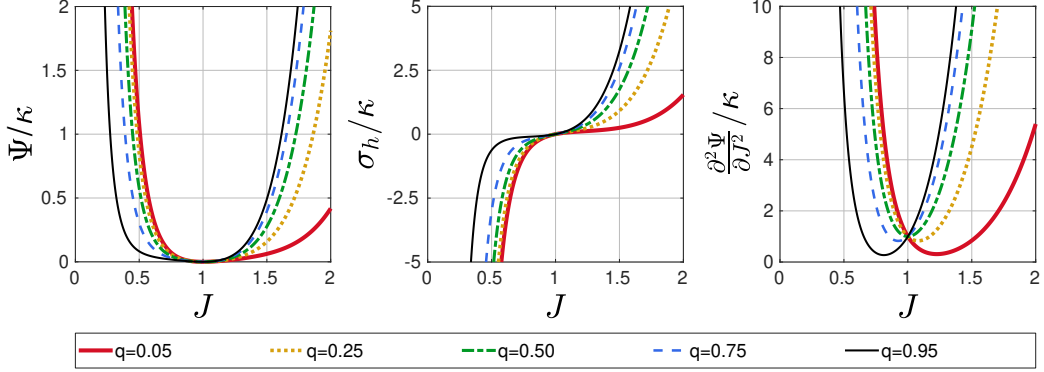


Figure A.25: The effect of q . The normalized strain energy density (left), hydrostatic stress (middle), and tangent modulus (right) for formulation 1. Curves drawn for $J = [0, 2]$, $\kappa = 1$, $\beta_1 = 2$, $\beta_2 = 4$, $q = [0.05, 0.95]$.

747 However, it was found that a negative tangent may occur when q is altered
 748 to severely favour a particular domain (e.g. q close to 0 or 1) while β
 749 parameter for the "suppressed" domain is very high. This is illustrated in
 750 Figure A.26 where the combination $q = 0.05$ and $\beta_1 = 30$ (black curve in the
 751 left graph of Figure A.26), or $q = 0.95$ and $\beta_2 = 30$ (red curve in the right
 752 graph of Figure A.26), resulted in a negative tangent.

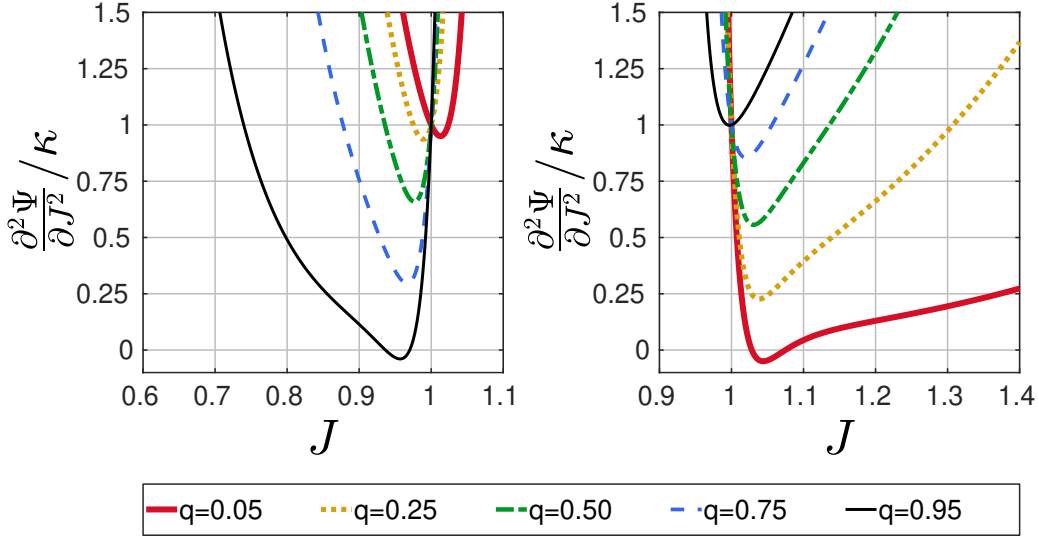


Figure A.26: The normalized tangent modulus when $\kappa = 1$, $q = [0.05, 0.95]$ and $\beta_1 = 30$, $\beta_2 = 3$ (left), or $\beta_1 = 3$, $\beta_2 = 30$ (right).

753 *Appendix A.2. Formulation 1 with a switch statement*

754 A second variation on formulation 1 is now presented which contains a
 755 switch statement to fully uncouple the behaviour for shrinkage and expansion:

$$\Psi_{vol}(J) = \frac{\kappa}{2} \begin{cases} \frac{1}{\beta_1^2} (J^{\beta_1} - 1)^2 & J \geq 1 \\ \frac{1}{\beta_2^2} (J^{-\beta_2} - 1)^2 & J < 1 \end{cases} \quad (\text{A.4})$$

756 Leading to the following expression for the hydrostatic stress:

$$\sigma_h(J) = \frac{\kappa}{J} \begin{cases} \frac{1}{\beta_1} (J^{2\beta_1} - J^{\beta_1}) & J \geq 1 \\ \frac{1}{\beta_2} (J^{-2\beta_2} - J^{-\beta_2}) & J < 1 \end{cases} \quad (\text{A.5})$$

757 and the tangent modulus:

$$\frac{\partial^2 \Psi_{vol}(J)}{\partial J^2} = \frac{\kappa}{J^2} \begin{cases} \frac{1}{\beta_1} \left((2\beta_1 - 1)J^{2\beta_1} - (\beta_1 - 1)J^{\beta_1} \right) & J \geq 1 \\ \frac{1}{\beta_2} \left((2\beta_2 + 1)J^{-2\beta_2} - (\beta_2 + 1)J^{-\beta_2} \right) & J < 1 \end{cases} \quad (\text{A.6})$$

758 This "switch-based" variation performs similarly to formulation 1 of sec-
 759 tion 4.1 but enables fully separated control of the expansion and shrinkage
 760 behaviour. Figure A.27 illustrates the effect of varying β_1 (since similar
 761 performance is obtained for β_2 these graphs are not shown here). Clearly
 762 fully independent control of strain hardening for the expansion and shrink-
 763 age domains is achieved. Furthermore, by using the conditional switch, the
 764 minimum stiffness is guaranteed to be κ and lies at $J = 1$. However, the
 765 switch-based implementation presents with a potentially undesired artefact
 766 in the form of a non-smooth transition at $J = 1$ for the tangent modulus (see
 767 the kink at $J = 1$ for the tangent graphs of Figure A.27).

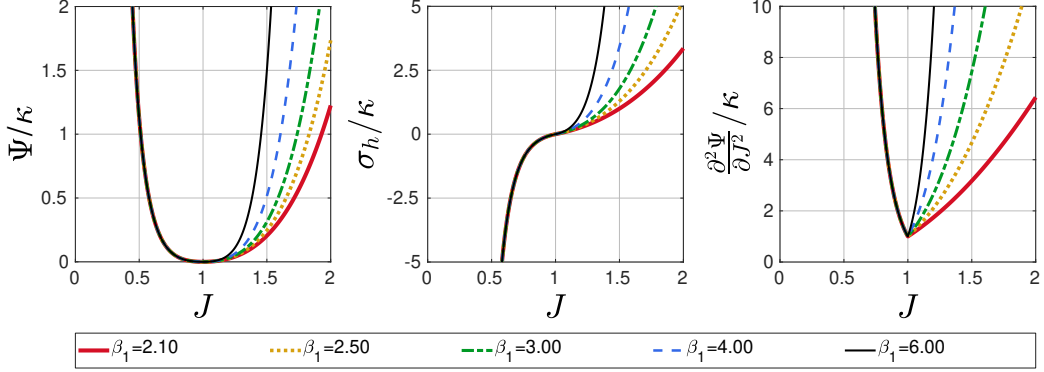


Figure A.27: The effect of β_1 . The normalized strain energy density (left), hydrostatic stress (middle), and tangent modulus (right) for formulation 1. Curves drawn for $J = [0, 2]$, $\kappa = 1$, $\beta_2 = 2$, $\beta_1 = [2.1, 6]$.

768 *Appendix A.3. Formulation 2 without asymptote parameters*

769 This variation is a hybrid between equation 7 and formulation 2 is pro-
770 posed:

$$\Psi_{vol}(J) = \kappa \begin{cases} \frac{1}{\beta_1^2} (\cosh(\beta_1(J-1)) - 1) & J \geq 1 \\ \frac{1}{2} \left[\frac{1}{\beta_2^2} (\cosh(\beta_2(J-1)) - 1) - \frac{4}{\pi^2} \ln(\cos(\frac{\pi}{2}(1+J))) \right] & J < 1 \end{cases} \quad (A.7)$$

771 Resulting in the following expression for the hydrostatic stress:

$$\sigma_h(J) = \kappa \begin{cases} \frac{1}{\beta_1} \sinh(\beta_1(J-1)) & J \geq 1 \\ \frac{1}{2} \left[\frac{1}{\beta_2} \sinh(\beta_2(J-1)) - \frac{2}{\pi} \tan(\frac{\pi}{2}(1+J)) \right] & J < 1 \end{cases} \quad (A.8)$$

772 and the tangent:

$$\frac{\partial^2\Psi_{vol}(J)}{\partial J^2} = \kappa \begin{cases} \cosh(\beta_1(J-1)) & J \geq 1 \\ \frac{1}{2} \left[\cosh(\beta_2(J-1)) + \sec^2(\frac{\pi}{2}(1+J)) \right] & J < 1 \end{cases} \quad (A.9)$$

773 Here β_1 and β_2 are material parameters controlling volumetric strain-dependent
774 stiffening. As equation A.7 shows both the shrinkage and expansion domain

775 feature a form equivalent to equation 7. However, to adhere to criteria *V*
 776 and *VI* of Table 1 a term similar to equation 20 (with $a(J_2 = 0)$) such that a
 777 fixed asymptote occurs at $J = 0$) is added for the shrinkage domain.

778 Figure A.28 and Figure A.29 illustrate the effect of varying the β_1 and
 779 β_2 .

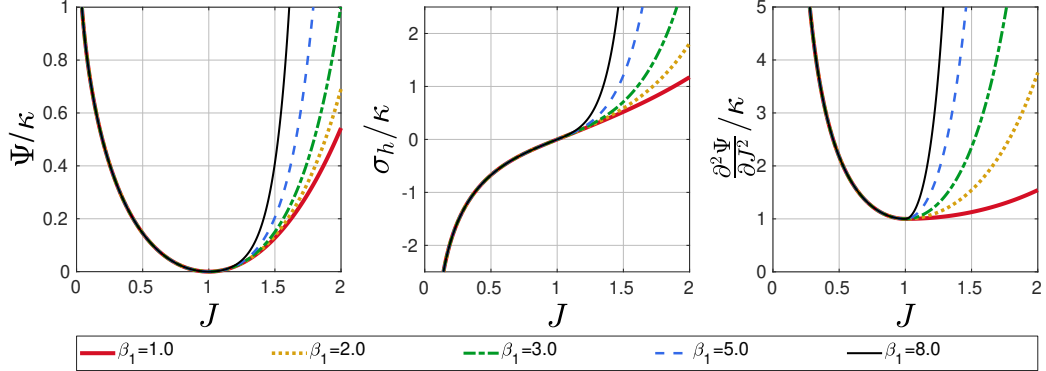


Figure A.28: The effect of β_1 . The normalized strain energy density (left), hydrostatic stress (middle), and tangent modulus (right) for formulation 2. Curves drawn for $J = [0, 2]$, $\kappa = 1$, $\beta_2 = 3$, $\beta_1 = [1, 12]$.

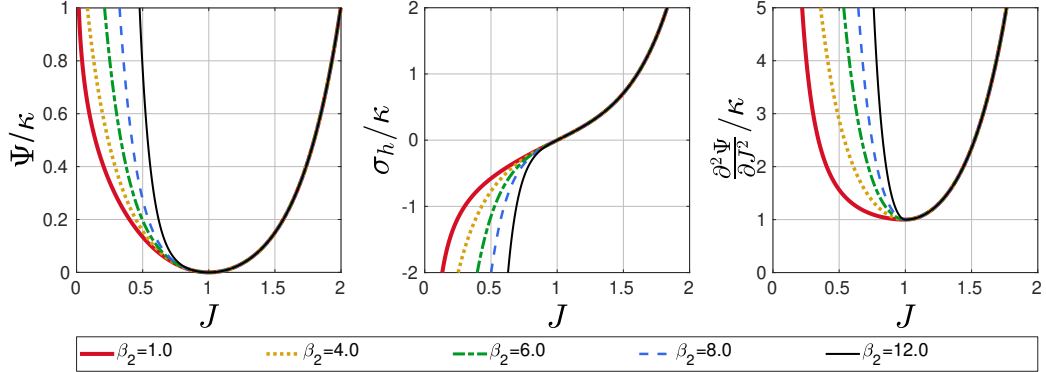


Figure A.29: The effect of β_2 . The normalized strain energy density (left), hydrostatic stress (middle), and tangent modulus (right) for formulation 2. Curves drawn for $J = [0, 2]$, $\kappa = 1$, $\beta_1 = 3$, $\beta_2 = [1, 12]$.

780 The graphs of Figure A.28 and Figure A.29 show fully independent control
 781 of the strain stiffening for shrinkage and expansion. This variation adheres
 782 to all criteria of Table 1. The minimum tangent occurs at $J = 1$, where,

⁷⁸³ since the third derivatives for the shrinkage and expansion terms of equation
⁷⁸⁴ A.7 are both zero, a smooth transition occurs between the two domains.